Article

Immunity

Single-cell multiomics reveals persistence of HIV-1 in expanded cytotoxic T cell clones

Graphical abstract

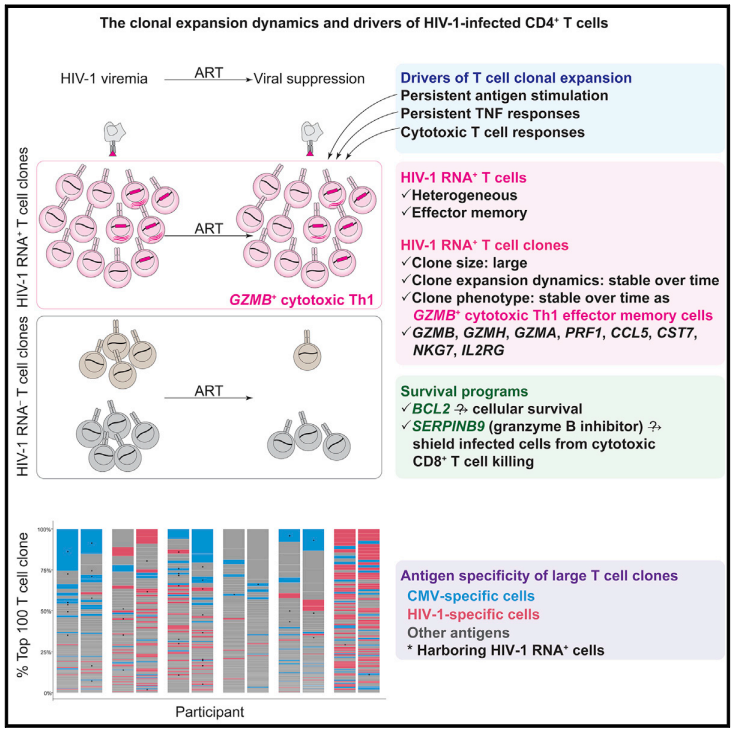

Highlights

- Most HIV-1 RNA$^+$ T cell clones are large, stable, *GZMB*$^+$ cytotoxic effector memory Th1s
- Some HIV-1 RNA$^+$ cells express *SERPINB9* and may be shielded from CD8$^+$ T cell killing
- Antigen stimulation, TNF, and cytotoxic T cell responses determine T cell clone size
- Early ART cannot fully reduce chronic immune activation, and TNF responses persist

Authors

Jack A. Collora, Runxia Liu, Delia Pinto-Santini, ..., David van Dijk, Ann Duerr, Ya-Chi Ho

Correspondence

ya-chi.ho@yale.edu

In brief

Using single-cell ECCITE-seq, Collora et al. profiled 267 HIV-1 RNA$^+$ cells and 68 expanded HIV-1 RNA$^+$ T cell clones from 215,458 CD4$^+$ T cells. HIV-1 resides in *GZMB*$^+$ cytotoxic Th1 effector memory CD4$^+$ T cell clones that are large and persistent. HIV-1-infected cytotoxic CD4$^+$ T cells may evade cytotoxic CD8$^+$ T cell killing through Seprin B9 degradation of granzyme B.

Collora et al., 2022, Immunity *55*, 1–19
June 14, 2022
https://doi.org/10.1016/j.immuni.2022.03.004

CellPress

Please cite this article in press as: Collora et al., Single-cell multiomics reveals persistence of HIV-1 in expanded cytotoxic T cell clones, Immunity (2022), https://doi.org/10.1016/j.immuni.2022.03.004

Immunity

CellPress

Article

Single-cell multiomics reveals persistence of HIV-1 in expanded cytotoxic T cell clones

Jack A. Collora,[1] Runxia Liu,[1] Delia Pinto-Santini,[2] Neal Ravindra,[3,4] Carmela Ganoza,[5] Javier R. Lama,[5] Ricardo Alfaro,[6] Jennifer Chiarella,[7] Serena Spudich,[7] Karam Mounzer,[8] Pablo Tebas,[9] Luis J. Montaner,[10] David van Dijk,[3,4] Ann Duerr,[2] and Ya-Chi Ho[1,11,*]

[1]Department of Microbial Pathogenesis, Yale University School of Medicine, New Haven, CT 06519, USA
[2]Vaccine and Infectious Disease, Fred Hutchinson Cancer Research Center, Seattle, WA, 98109, USA
[3]Department of Internal Medicine (Cardiology), Yale School of Medicine, New Haven, CT 06520, USA
[4]Department of Computer Science, Yale University, New Haven, CT 06520, USA
[5]Asociación Civil Impacta Salud y Educación, Lima, 15063, Perú
[6]Centro de Investigaciones Tecnológicas Biomédicas y Medioambientales (CITBM), Lima, 07006, Perú
[7]Department of Neurology, Yale University School of Medicine, New Haven, CT 06519, USA
[8]Philadelphia FIGHT Community Health Centers, Philadelphia, PA 19107, USA
[9]Department of Medicine, University of Pennsylvania, Philadelphia, PA 19104, USA
[10]The Wistar Institute, Philadelphia, PA 19104, USA
[11]Lead contact
*Correspondence: ya-chi.ho@yale.edu
https://doi.org/10.1016/j.immuni.2022.03.004

SUMMARY

Understanding the drivers and markers of clonally expanding HIV-1-infected CD4$^+$ T cells is essential for HIV-1 eradication. We used single-cell ECCITE-seq, which captures surface protein expression, cellular transcriptome, HIV-1 RNA, and TCR sequences within the same single cell to track clonal expansion dynamics in longitudinally archived samples from six HIV-1-infected individuals (during viremia and after suppressive antiretroviral therapy) and two uninfected individuals, in unstimulated conditions and after CMV and HIV-1 antigen stimulation. Despite antiretroviral therapy, persistent antigen and TNF responses shaped T cell clonal expansion. HIV-1 resided in Th1-polarized, antigen-responding T cells expressing *BCL2* and *SERPINB9* that may resist cell death. HIV-1 RNA$^+$ T cell clones were larger in clone size, established during viremia, persistent after viral suppression, and enriched in *GZMB*$^+$ cytotoxic effector memory Th1 cells. Targeting HIV-1-infected cytotoxic CD4$^+$ T cells and drivers of clonal expansion provides another direction for HIV-1 eradication.

INTRODUCTION

Despite effective antiretroviral therapy (ART), the HIV-1 latent reservoir (Chun et al., 1997; Finzi et al., 1997; Wong et al., 1997) persists lifelong (Crooks et al., 2015; Siliciano et al., 2003). More than 50% of the HIV-1 latent reservoir is maintained by clonal expansion of infected cells (Bui et al., 2017; Hosmane et al., 2017; Lorenzi et al., 2016). Clonally expanding HIV-1-infected cells are established during acute viremia (Coffin et al., 2019) and persist under long-term suppressive ART (Maldarelli et al., 2014; Wagner et al., 2014). The clonal expansion of HIV-1-infected cells is a major barrier to cure. Understanding the drivers and markers of clonally expanding HIV-1-infected cells is essential for HIV-1 eradication.

The clonal expansion of HIV-1-infected cells is driven by antigen stimulation, homeostatic proliferation (Chomont et al., 2009), and HIV-1-driven cancer gene expression (Liu et al., 2020; Maldarelli et al., 2014; Mellors et al., 2021; Wagner et al., 2014). Upon cognate antigen stimulation, T cells can proliferate into a T cell clone of many cells that share the same T cell receptor (TCR) sequence and antigen specificity. HIV-1 can reside in cytomegalovirus (CMV)-specific (Mendoza et al., 2020; Simonetti et al., 2021), HIV-1-specific (Douek et al., 2002; Mendoza et al., 2020; Simonetti et al., 2021), and cancer-specific CD4$^+$ T cells (Simonetti et al., 2016) that are clonally expanding. Presumably, antigen stimulation and cytokines that drive the proliferation of a T cell clone would also drive the proliferation of HIV-1-infected cells within this T cell clone. Unlike homeostatic proliferation, which does not induce HIV-1 reactivation (Bosque et al., 2011; Wang et al., 2018), antigen stimulation can induce HIV-1 reactivation and viral protein expression from the clonally expanding HIV-1-infected cells and cause persistent low-level viremia despite ART (Bailey et al., 2006; Halvas et al., 2020). However, upon antigen stimulation, cells harboring inducible HIV-1 should presumably die of viral cytopathic effects or T cell activation. It remains unclear why HIV-1-infected cells can resist cell death upon reactivation and persist over time.

Antigen-specific CD4$^+$ T cells are susceptible to HIV-1 infection (Douek et al., 2002; Mendoza et al., 2020; Simonetti et al., 2021). Among antigen-specific CD4$^+$ T cells, cytotoxic

Please cite this article in press as: Collora et al., Single-cell multiomics reveals persistence of HIV-1 in expanded cytotoxic T cell clones, Immunity (2022), https://doi.org/10.1016/j.immuni.2022.03.004

$CD4^+$ T cells are key effectors in cancer (Malandro et al., 2016; Oh et al., 2020) and viral infections, such as influenza (Brown et al., 2012), CMV (van Leeuwen et al., 2004), and SARS-CoV-2 infections (Meckiff et al., 2020). In HIV-1-infected individuals, cytotoxic $CD4^+$ T cells are substantially expanded during HIV-1 infection (Appay et al., 2002) and CMV infection (Zaunders et al., 2004). Cytotoxic $CD4^+$ T cells have a high proliferative capacity and exhibit polyfunctional cytotoxic responses through release of cytolytic granules [such as granzyme B (*GZMB*), granzyme K (*GZMK*), granzyme H (*GZMH*), and perforin (*PRF1*)] and expression of T helper 1 (Th1) cytokines [interferon (IFN)-γ, interleukin (IL)-2, and tumor necrosis factor (TNF)] (Appay et al., 2002). Unlike cytotoxic $CD8^+$ T cells which can control HIV-1 infection, the role of cytotoxic $CD4^+$ T cells in HIV-1 infection remains unclear.

ART suppresses HIV-1 plasma viral load to clinically undetectable levels. However, ART neither kills infected cells nor inhibits HIV-1 viral protein production from existing infected cells. Therefore, HIV-1-infected cells can continue to produce viral antigens (Halvas et al., 2020; Pollack et al., 2017) and induce immune activation and exhaustion (Bengsch et al., 2018; Pollack et al., 2017). Early ART initiated within 6 months of infection, as opposed to deferred ART initiated after 6 months of infection, substantially reduces chronic immune activation (Jain et al., 2013). Given that people treated with immediate ART have a shorter duration of HIV-1 viremia, shorter duration of overt HIV-1 antigen exposure, and lower levels of immune activation (Jain et al., 2013), comparing immune responses in people treated after short versus long duration of viremia may help to understand HIV-1-specific immune responses under different magnitude of HIV-1 antigen stimulation *in vivo*.

Several challenges prevent mechanistic understanding of HIV-1 persistence in people with HIV-1. First, infected cells harboring intact and inducible HIV-1 proviruses in ART-treated individuals are extremely rare, accounting for <0.001% of $CD4^+$ T cells in the peripheral blood (Bruner et al., 2016; Bruner et al., 2019; Ho et al., 2013). Second, there are no known cellular markers that can exclusively differentiate HIV-1-infected cells from uninfected cells, given the heterogeneity (Neidleman et al., 2020) in polarization (Lee et al., 2017), activation state (Lee et al., 2019), memory differentiation (Gantner et al., 2020; Hiener et al., 2017; Venanzi Rullo et al., 2020), and immune exhaustion states (Fromentin et al., 2016). Third, while HIV-1-infected cells can be isolated using viral markers such as HIV-1 RNA expression (Liu et al., 2020) or Env protein expression (Cohn et al., 2018), these methods require *ex vivo* activation and thus cannot depict the *in vivo* status of infected cells. Advancements in single-cell technologies enable high-dimensional immune profiling to dissect the heterogeneous states of immune cells, capture rare cells, map T cell clonality, and identify upstream drivers of immune dysregulation (Hoang et al., 2021; Kazer et al., 2020; Nguyen et al., 2019; Shalek et al., 2013; Wilk et al., 2020; Yost et al., 2019). Further, computational techniques including supervised and unsupervised machine learning, network analysis, and statistical methodologies enable confident identification of higher-fidelity predictors of different cellular states from the sparse and highly complex single-cell multi-modal data (Hu et al., 2016; Langfelder and Horvath, 2008; Pappalardo et al., 2020; Park et al., 2020; Stuart et al., 2019; Torang et al., 2019). Single-cell genome-wide transcriptome profiling can resolve the heterogeneity of immune cells, identify the rare HIV-1-infected cells, and discover mechanisms of HIV-1 persistence.

We hypothesize that HIV-1 persists by residing in $CD4^+$ T cells that are proliferative, resistant to cell death, and persistent over time. We reasoned that immune drivers that determine the proliferation of T cell clones will also drive the proliferation of HIV-1-infected cells within these T cell clones. Here, we use a single-cell multiomic approach to track $CD4^+$ T cell immune responses during acute HIV-1 infection and after viral suppression, both in unstimulated *in vivo* states and after *ex vivo* antigen stimulation. We examined the transcriptional landscape, immune regulators, and T cell clonal expansion dynamics of T cell clones and HIV-1 RNA^+ cells. We identified HIV-1-induced immune dysfunction, $CD4^+$ T cell responses to antigen stimulation, drivers of the clonal expansion of HIV-1 RNA^+ T cell clones, and the survival programs that prevent cell death upon HIV-1 reactivation and T cell activation.

RESULTS

Single-cell ECCITE-seq captures immune phenotype, HIV-1 RNA expression, and T cell clonality in the same single cell

To understand the impact of HIV-1 infection on $CD4^+$ T cell immune responses, T cell clonal expansion dynamics, and HIV-1 persistence, we examined the transcriptome, surface protein expression, T cell clonality, and HIV-1 expression in total $CD4^+$ T cells from six HIV-1-infected individuals at the single cell level. We used single-cell expanded CRISPR-compatible cellular indexing of transcriptomes and epitopes by sequencing (ECCITE-seq), which captures surface protein expression, cellular transcriptome, HIV-1 RNA, and TCR sequence within the same single cell. This allows us to track the clonal expansion dynamics using longitudinally archived samples. We used longitudinally archived blood samples from the Sabes study (Lama et al., 2018; Lama et al., 2021), a prospective study that tested HIV-1 status monthly to identify early infection. We profiled paired $CD4^+$ T cells at two time points, during viremia (<60 days within estimated date of detectable infection [EDDI]) and after viral suppression (one year of suppressive ART, with >6 months of undetectable viral load), in six HIV-1-infected individuals (Figures 1A and S1; Table S1). $CD4^+$ T cells from two uninfected individuals served as controls. Notably, the uninfected individuals were recruited based on availability and matched with sex but not age or ethnicity. Our data would need to be cautiously interpretated as age and ethnicity may affect the immune profiles (Barreiro and Quintana-Murci, 2010; King Thomas et al., 2019).

We profiled 89,279 $CD4^+$ T cells from six infected individuals, including 52,473 during viremia and 36,806 after viral suppression, and compared them with 33,406 cells from two uninfected individuals. Batch effects were removed using fast mutual nearest neighbors correction (fastMNN) (Haghverdi et al., 2018) (Figures 1A and S2). Cells were clustered and visualized based on their transcriptome profile using Uniform Manifold Approximation and Projection for Dimension Reduction (UMAP) (Becht et al., 2018). For each sample, we identified a median of 7,447 cells, with a median of 1,346 genes and 4,138 unique molecular identifiers (UMI) in each cell (Table S2).

Please cite this article in press as: Collora et al., Single-cell multiomics reveals persistence of HIV-1 in expanded cytotoxic T cell clones, Immunity (2022), https://doi.org/10.1016/j.immuni.2022.03.004

CellPress

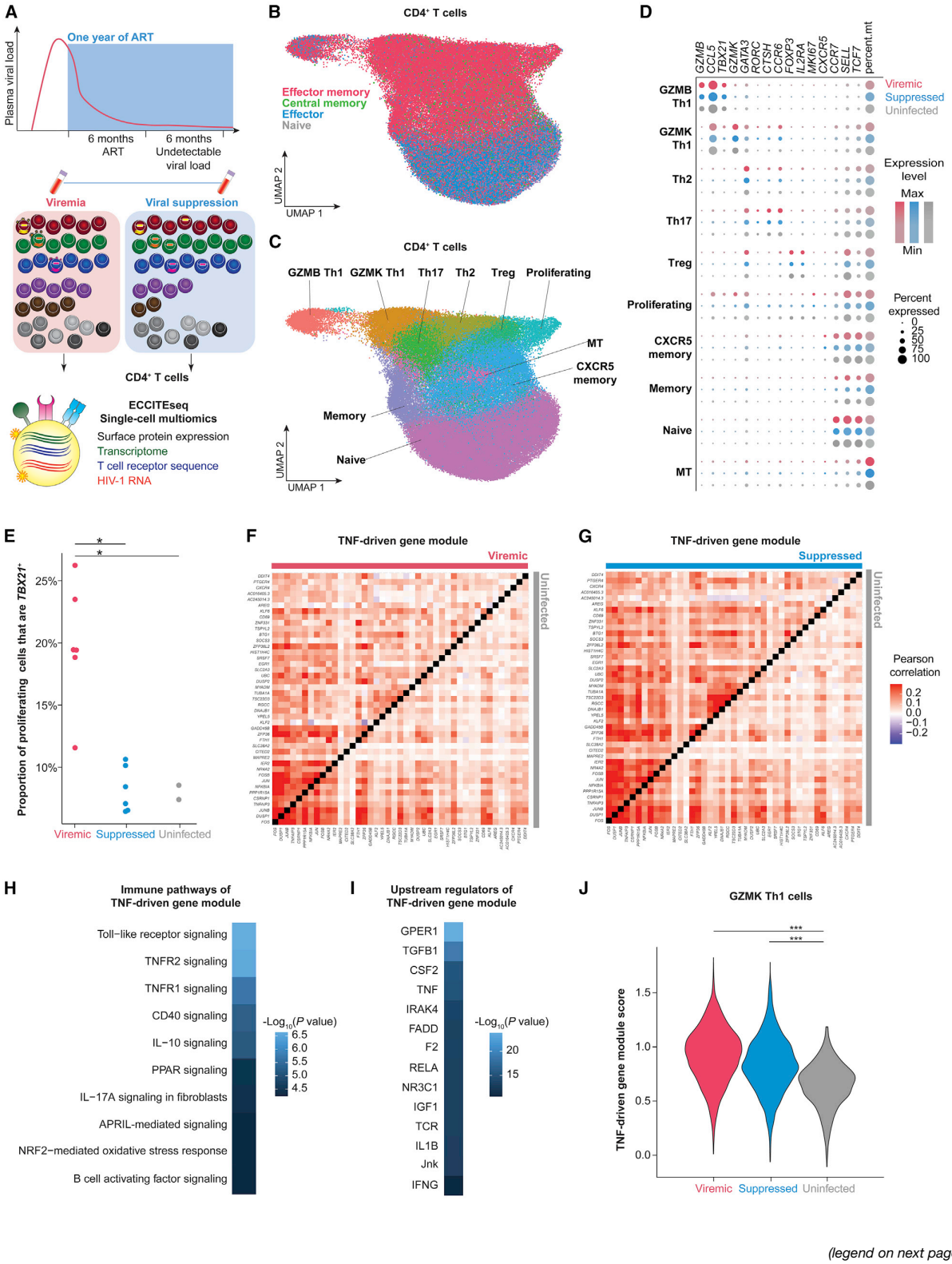

(legend on next page)

Please cite this article in press as: Collora et al., Single-cell multiomics reveals persistence of HIV-1 in expanded cytotoxic T cell clones, Immunity (2022), https://doi.org/10.1016/j.immuni.2022.03.004

We determined the memory phenotype of each cell based on their surface CD45RA and CCR7 protein expression and identified naive, central memory, effector memory, and effector $CD4^+$ T cells (Figure 1B). Surface protein expression was determined as positive by $>90^{th}$ percentile of the expression level of isotype barcoded antibody controls. Based on cellular transcriptome and surface marker expression, we defined ten clusters including two of cytotoxic Th1 cells (GZMB Th1 and GZMK Th1), Th2, Th17, Treg, proliferating, two of memory cells, naive, and a high mitochondrial gene expression (MT) (Figures 1C, 1D, and S2; Table S2). In the proliferating cell cluster, there were more cells expressing the Th1 polarization transcription factor *TBX21* during viremia than in suppressed and uninfected conditions, suggesting that proliferation of Th1 cells was most prominent during viremia (Figure 1E).

TNF responses persist despite ART and shape Th1 responses

To understand how HIV-1-induced immune dysfunction shapes the $CD4^+$ T cell immune responses, we identified co-regulated genes that could distinguish the immune responses between viremia, viral suppression, and uninfected conditions using *de novo* gene set identification. Using weighted gene correlation network analysis (WGCNA) (Langfelder and Horvath, 2008), we identified nine consensus sets (modules) of genes that could distinguish gene expression differences between viremia, viral suppression, and uninfected conditions. We found that a proliferation module (Figures S2G–S2L), a GZMB-Treg module (Figures S2M–S2R), and a TNF signaling module (Figures 1F–1J) that distinguished viremia, viral suppression, and uninfected conditions (Figure S2). The proliferation module and GZMB-Treg module increased gene expression during viremia but returned to normal levels after viral suppression (Figure S2), reflecting the peak of host immune responses to acute viral infection. We found that the TNF signaling module was induced during viremia (Figure 1F) and persisted despite viral suppression (Figure 1G). Using Ingenuity Pathway Analysis (IPA), we found that genes in the TNF signaling module were enriched for pathways for signaling via TNF receptors, toll-like receptor, and CD40 (Figure 1H). The upstream drivers of the TNF signaling module included transforming growth factor β (TGFβ), TNF, T cell activation, IL-1β, and IFN-γ (Figure 1I). When we examined the TNF signaling module score, the aggregate normalized expression levels of these genes, we found that TNF signaling gene expression in GZMK Th1 was significantly higher during viremia and remained elevated after viral suppression relative to uninfected individuals (Figure 1J).

We next examined the impact of immediate versus deferred ART on immune responses (Figure S3). We found that immediate versus deferred ART modestly impacted memory cell phenotypes (Figure S3A) and T cell polarization (Figure S3B). Th1 proliferation was not significantly different after immediate versus deferred ART (Figure S3C). We identified a TNF-driven gene module that was expressed at significantly higher levels in the deferred ART group than the immediate ART group (Figures S3D–S3F), particularly in the Th2 and CXCR5 memory cell populations but not in the GZMK Th1 population (Figures S3G–S3O). Our results suggest ART can reduce but cannot fully block HIV-1-induced immune activation. Cytokines such as TNF and TGFβ continue to shape Th1 responses despite suppressive ART.

The clonal expansion dynamics of cytotoxic Th1 $CD4^+$ T cells are shaped by antigen and TNF responses

We then investigated how cytokine responses impacted T cell clonal expansion dynamics during HIV-1 infection. Inflammatory cytokines impact clonal expansion and differentiation of antigen-specific $CD4^+$ T cells (Pape et al., 1997). T cell clones can be identified based on their shared TCR sequences: cells having identical TCR sequences presumably originate from the same T cell that proliferated into a T cell clone in response to the same antigen stimulation (Figure 2A). We profiled the TCR repertoire using bulk TCR sequencing in addition to single-cell TCR sequences captured in ECCITE-seq to determine T cell clone size with greater precision. In all, we profiled 1,118,713 TCR sequences (median of 57,778 TCR sequences per sample per time point) and identified 8,268 single cells in T cell clones (median of 575 cells per sample per time point).

We found that the most clonal clusters, as measured by the Gini index (Gillet et al., 2011), were proliferating cells and polarized effector memory cells, including GZMB Th1, GZMK Th1, Th2, Th17, and Treg clusters (Figure 2B). These T cell clusters were significantly more clonal than naive cells (Figure 2C). Among them, the most clonal T cell cluster was the GZMB Th1 cells (Figure 2C).

Figure 1. Paired $CD4^+$ T cell profiling during viremia and after viral suppression by single-cell multiomic ECCITE-seq reveals persistent TNF responses despite suppressive ART

(A) Study design. Participants enrolled in the Sabes study were prospectively tested monthly for HIV-1 infection using HIV-1 antibody detection, antigen detection, and viral RNA quantification. We profiled paired $CD4^+$ T cells during acute viremia (<60 days after estimated date of detectable infection) and after one year of suppressive ART (with documented undetectable viral load 6 months prior to the viral suppression time point) from 6 HIV-1-infected individuals enrolled in Sabes and subsequently followed in the Merlin study. $CD4^+$ T cells from 2 sex-matched uninfected individuals were used as controls.

(B) UMAP plot of memory phenotypes of cells (n = 52,473, 36,806, and 33,406 cells in the viremic, virally suppressed, and uninfected conditions, respectively) defined by surface CD45RA and CCR7 expression.

(C) UMAP of 10 clusters of $CD4^+$ T cells defined by transcriptome. (D) Dot plot depicting key cluster marker expression in viremic, suppressed, and uninfected conditions.

(E) The proportion of proliferating cells expressing *TBX21*, the key transcription factor for Th1 polarization. p values were determined by Wilcoxon rank-sum test.

(F and G) Pearson's correlation coefficient heatmaps of TNF-driven gene expression module of viremia versus uninfected conditions (F) and suppressed versus uninfected conditions (G).

(H and I) Ingenuity pathway analysis (IPA) heatmaps of enriched immune pathways (H) and predicted upstream regulators (I) of the TNF-driven gene expression module. p values were defined by Fisher's exact test.

(J) Module score of TNF-driven gene expression module in viremia, viral suppression, and uninfected conditions in the Th1 polarized GZMK cluster. p values were determined by Wilcoxon rank-sum test comparing HIV-1-infected conditions and uninfected conditions.

*$p < 0.05$; ***$p < 0.0001$. p values were corrected for multiple comparisons using the Benjamini-Hochberg procedure. See also Figures S1–S3; Tables S1 and S2.

Please cite this article in press as: Collora et al., Single-cell multiomics reveals persistence of HIV-1 in expanded cytotoxic T cell clones, Immunity (2022), https://doi.org/10.1016/j.immuni.2022.03.004

CellPress

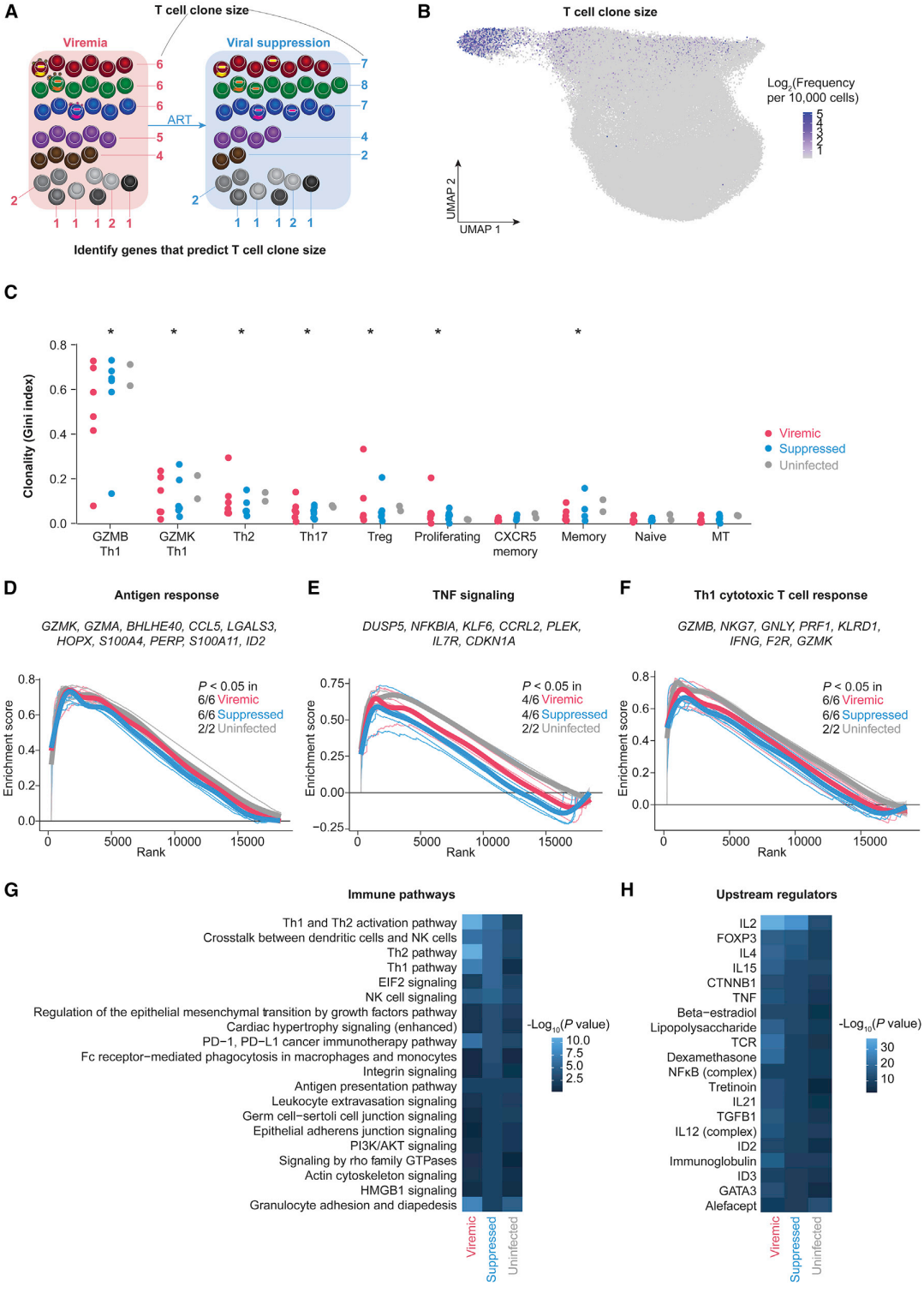

(legend on next page)

Please cite this article in press as: Collora et al., Single-cell multiomics reveals persistence of HIV-1 in expanded cytotoxic T cell clones, Immunity (2022), https://doi.org/10.1016/j.immuni.2022.03.004

To identify cellular transcriptional programs that correlate with T cell clone size, we ranked genes based on their correlation with T cell clone size in each participant at each time point, from those most correlated with a large clone size to those most correlated with a small clone size. Using this rank, we identified the immune pathways correlated with T cell clone size using gene set enrichment analysis (GSEA; Table S3). We identified three pathways that are positively associated with T cell clone size: antigen responses (Figure 2D), TNF signaling (Figure 2E), and Th1 cytotoxic responses (Figure 2F). Of note, these pathways were not different between immediate versus deferred ART (Figures S3K–S3M). Our finding suggests that despite suppressive ART, antigen responses and TNF signaling continue to shape T cell clonal size.

To identify genes that predict T cell clone size, we used elastic net regression (Zhou and Hastie, 2005) to analyze gene expression level and T cell clone size across participants in each condition. Elastic net regression is a machine-learning method that weights each gene according to how efficiently it predicts clone size and eliminates genes that are weakly or not predictive of clone size. We identified 444, 672, and 283 genes that predicted T cell clone size in viremic, suppressed, and uninfected conditions, respectively. We found that genes involving Th1, Th2, and crosstalk with dendritic cells and NK cells predicted T cell clone size in HIV-1-infected individuals, both during viremia and after viral suppression (Figure 2G). Using IPA, we found that the expression of these genes was driven by T cell polarization molecules (such as IL-2, IL-4, TNF, TGF, and IL-21), T cell activation, and homeostatic cytokines (Figure 2H). Overall, we found that T cell polarization and activation predicted T cell clonality both in HIV-1-infected and in uninfected individuals. However, T cell polarization and cytokine signaling had substantially higher impacts on T cell clonal expansion during HIV-1 infection (Figure 2G).

TCR repertoire mapping revealed distinct transcriptome programs of CMV-specific versus HIV-1-specific cells in unstimulated states

We wanted to examine whether HIV-1-induced antigen responses and TNF signaling during viremia and after viral suppression changed HIV-1 and CMV antigen responses. We isolated antigen-specific cells using the activation induced marker (AIM) assay (Dan et al., 2016; Morou et al., 2019). We used flow cytometry to sort CD69 and CD154 double-positive $CD4^+$ T cells as CMV-specific or HIV-1-specific $CD4^+$ T cells after nine hours of antigen stimulation (Figures 3A and S4A). Memory cells ($CD45RO^+$) that were double negative for CD69 and CD154 were sorted for comparison. We profiled $CD4^+$ T cells from the same six HIV-1-infected individuals during viremia and suppression using blood samples from the same time point. Using ECCITE-seq, we examined a total of 78,193 $CD4^+$ T cells, with 6,091 CMV-specific cells, 12,183 HIV-1-specific cells, and 59,919 memory cells. The frequency of CMV-specific and HIV-1-specific cells (Figure S4B) was not significantly different between conditions and was comparable to the frequency in previous reports (Morou et al., 2019; Simonetti et al., 2021). We used fastMNN to correct for batch effects (Figure S1). Antigen stimulated cells were mainly effector memory $CD4^+$ T cells (Figure 3B). We identified 15 clusters based on transcriptome differences (Figures 3C, S2, and S4C).

While not mutually exclusive, antigen-specific cells clustered distinctly from memory cells (Figure 3D). Antigen-specific cells were over-represented in 5 clusters: GZMB Th1, IL-2 Th1, activated Th1, lymphotoxin Th1, and CD45RA clusters (Figure 3E). In particular, the GZMB Th1 cells were mainly comprised of CMV-specific cells, while few HIV-1-specific cells were polarized into the GZMB Th1 phenotype. Although both CMV-specific and HIV-1-specific $CD4^+$ T cells were activated upon antigen stimulation, fewer HIV-1-specific cells upregulated Th1 and cytotoxic effector molecules (such as *IL2*, *TNF*, *IFNG*, *LTA*, *LTB*, *GZMB*, and *GNLY*) in the polarized Th1 clusters GZMB Th1 and IL-2 Th1 (Figure 3F). This suggests that Th1-polarized HIV-1-specific cells have less robust cytotoxic T cell responses compared with CMV-specific $CD4^+$ T cells. We found that the GZMB Th1 cells (mostly CMV-specific $CD4^+$ T cells) and the GZMB/H Th1 cells (mostly memory cells) were the most clonal cells both during viremia and after viral suppression (Figure 3G).

By identifying the TCR sequence of antigen-specific cells and tracking back to $CD4^+$ T cells having the same TCR sequence in unstimulated conditions (T cell repertoire overlap), we identified the unstimulated states of antigen-specific $CD4^+$ T cells. We found that GZMB/H Th1 cells during antigen stimulation, which were mainly memory cells not responding to CMV and HIV-1 antigen stimulation, were GZMB Th1 cells in the unstimulated condition (Figure 3H). CMV-specific cells, mainly GZMB Th1 cells during antigen stimulation, were also GZMB Th1 cells in the unstimulated condition (Figure 3I). These GZMB/H and GZMB Th1 cells had the highest T cell clonality, suggesting high levels of proliferation *in vivo*. This suggests that CMV-specific cells and a subset of memory cells (with unknown antigen specificity) are

Figure 2. T cell clone size is determined by antigen response, TNF signaling, and Th1 cytotoxic response

(A) T cells sharing the same TCR in the same individual are identified as a T cell clone. T cell clone size is the frequency of T cells sharing the same TCR sequence out of all cells with detected TCR sequences. By calculating the correlation between T cell clone size and gene expression levels in individual cells, we can identify the determinants of T cell clone size.

(B) UMAP plot indicating the $\log_2$ bulk clone size of each cell based on TCRβ nucleotide CDR3 junction sequence per 10,000 $CD4^+$ T cells.

(C) The level of clonality (as measured by Gini index) in each cluster in viremic, suppressed, and uninfected conditions. p values were determined by Wilcoxon rank-sum test comparing each cluster to naive cells.

(D–F) To identify pathways correlating with T cell clone size, we first ranked genes based on their correlation with clones size and then used gene set enrichment analysis (GSEA). We identified pathways including Goldrath antigen response (D), Hallmark TNF signaling via NF-κB (E), and Bosco Th1 cytotoxic module (F). Representative leading-edge genes (the top genes enriched in each pathway) were shown in each panel. Thick lines indicate the mean enrichment score for each condition and thin lines indicate the enrichment score for each individual.

(G and H) Genes that were predictive of T cell clone size across cells in each condition were identified by elastic net regression. These genes were then examined by IPA to determine the immune pathways (G) and upstream regulators (H). p values were defined by Fisher's exact test.

p values were corrected for multiple comparisons using the Benjamini-Hochberg procedure. *$p < 0.05$. See also Figure S3 and Table S3.

Please cite this article in press as: Collora et al., Single-cell multiomics reveals persistence of HIV-1 in expanded cytotoxic T cell clones, Immunity (2022), https://doi.org/10.1016/j.immuni.2022.03.004

CellPress

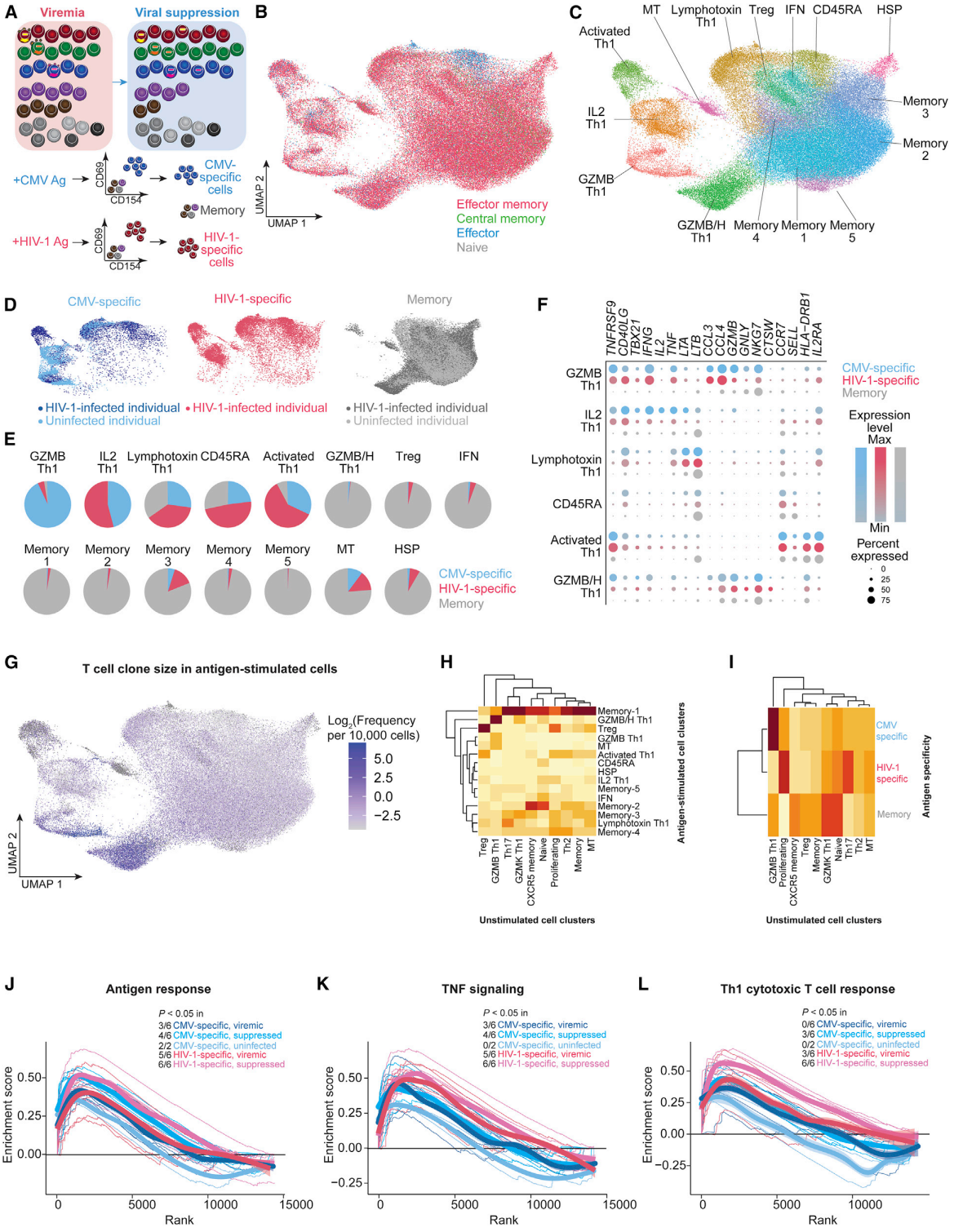

(legend on next page)

Please cite this article in press as: Collora et al., Single-cell multiomics reveals persistence of HIV-1 in expanded cytotoxic T cell clones, Immunity (2022), https://doi.org/10.1016/j.immuni.2022.03.004

polarized as GZMB Th1 cells in large clones both in unstimulated and stimulated conditions. In contrast, few HIV-1-specific CD4$^+$ T cells polarized as GZMB Th1 cells—HIV-1-specific CD4$^+$ T cells were mainly Th17 and proliferating T cells in unstimulated conditions (Figure 3I) and were less clonal (Figure 2C). Our results suggests that different antigen stimulation triggers different T cell polarization and proliferation.

TNF responses and cytotoxic T cell responses shape the clonal expansion of HIV-1-specific CD4$^+$ T cells after viral suppression

We examined the genes of which the expression levels correlate with T cell clone size in the antigen-stimulated cells. We found that antigen responses, TNF signaling, and cytotoxic T cell responses determine T cell clone size (Figures 3J–3L and S3J–S3O) as observed in the unstimulated condition (Figures 2D–2F). However, these responses varied depending on the antigen and the participant (Figure 3J–3L). Overall, we found that while antigen stimulation remains the major determinant of T cell clone size, T cell clonal expansion of HIV-1-specific cells is significantly affected by TNF signaling and cytotoxic T cell responses, particularly after viral suppression.

Prolonged viremia decreases GZMB Th1 effector cells

Comparing HIV-1-specific immune responses in individuals having shorter duration of viremia (in the immediate ART cohort, receiving ART in 30.3 days on average) versus longer duration of viremia (in the deferred ART cohort, receiving ART in 197.3 days on average; Figure S1; Table S1) allows us to examine the impact of prolonged HIV-1 antigen stimulation on HIV-1-specific CD4$^+$ T cells *in vivo*. Previous reports have shown that HIV-1-specific T cells display a different phenotype based on the time of ART initiation (Ndhlovu et al., 2019). We found that in HIV-1-spcific CD4$^+$ T cells, deferred ART decreased the proportion of GZMB/H Th1 cells (Figure S4C) and effector cells (Figure S4D). When we examined whether the gene expression profiles were different in each cluster between immediate versus deferred ART (Figures S4E–S4J), we found that in people receiving deferred ART, lymphotoxin Th1 cells had significantly lower levels of *IFNG* and *GZMB* expression (Figure S4G). Overall, prolonged viremia impairs HIV-1-specific CD4$^+$ T cells function by decreasing GZMB effector cell proportion and Th1 effector function.

HIV-1 RNA$^+$ cells are heterogeneous

We next wanted to examine the differences between HIV-1 RNA$^+$ cells and HIV-1 RNA$^-$ cells (Figure 4A). We mapped single-cell transcriptome reads to autologous HIV-1 proviral sequences and HXB2 reference. Mapping the transcriptome to autologous HIV-1 sequences increased mapping rate by approximately 20% and increased spliced HIV-1 RNA detection (Figure S5). Due to the 5′-biased RNA capture by ECCITE-seq, most HIV-1 RNA captured were near the 5′ LTR. We identified spliced HIV-1 RNA, mostly spliced from the major splice donor site. To guard against potential sequencing artifacts generated by index hopping, HIV-1 RNA$^+$ cells were defined by the presence of HIV-1 RNA having at least 2 UMIs (representing two unique reverse transcription events in the same single cell) or at least 4 reads of a single UMI. This threshold yielded no HIV-1 RNA$^+$ cells in samples from uninfected individuals. In unstimulated and virally suppressed conditions, HIV-1 RNA$^+$ cells indicated latency reversal *in vivo*. In the antigen-stimulated conditions, HIV-1 RNA$^+$ cells indicated HIV-1 latency reversal *ex vivo*. Of note, we found that the normalized expression levels of HIV-1 RNA in viremic, suppressed, unstimulated, and stimulated conditions were not significantly different (Figures S5C and S5D). Of note, HIV-1-infected cells that remained latent or had transcriptional defects might not be captured because of the lack of detectable HIV-1 RNA expression.

In the unstimulated samples, we identified 90 HIV-1 RNA$^+$ cells, including 81 from the viremic time point and 9 from the virally suppressed time point (Figure 4B). In the antigen-stimulated conditions, we identified 177 HIV-1 RNA$^+$ cells, including 134 during viremia and 43 during suppression (Figure 4C). Among them, 21 were CMV-specific cells, 28 were HIV-1-specific cells, and 128 were memory cells (Figure 4D). The majority of HIV-1 RNA$^+$ cells resided in memory cells, likely because more memory cells were profiled than antigen-specific cells. These memory cells would likely respond to antigens other than CMV and HIV-1. Despite transcriptome and clonal expansion differences

Figure 3. TCR repertoire mappings revealed the different transcriptome program of CMV-specific versus HIV-1-specific cells in unstimulated states

(A) CMV-specific and HIV-1-specific CD4$^+$ T cells were isolated as cells expressing both activation inducible markers (AIM) (CD69 and CD154) after 9 h of antigen stimulation in the presence of autologous CD8-depleted PBMC. CMV-specific cells, HIV-1-specific cells, and CD45RO$^+$ memory cells were sorted by flow cytometry for single-cell ECCITE-seq.

(B) UMAP plot of memory phenotypes of cells (n = 33,805, 44,388, and 14,580 cells in the viremic [from 6 individuals], viral suppression [from 6 individuals], and uninfected conditions [from 2 individuals], respectively) defined by surface CD45RA and CCR7 expression. These samples came from the same infected study participants and same time points as profiled in the unstimulated conditions. CD45RA and CCR7 positivity was determined by barcoded surface protein staining.

(C) UMAP plot of 15 transcriptionally defined clusters identified in the viremic, virally suppressed, and uninfected conditions.

(D) UMAP plots of cells split across CMV-specific (n = 6,091), HIV-1-specific (n = 12,183), and sorted memory cell populations (n = 59,919).

(E) Proportion of each cluster grouped by antigen specificity, with 5 clusters predominantly antigen responsive.

(F) Dot plot of key effector gene expression across antigen-specific conditions in antigen-specific clusters.

(G) UMAP plot indicating the T cell clone size of each cell based on TCRβ nucleotide CDR3 junction sequence per 10,000 CD4$^+$ T cells.

(H) Heatmap indicating the proportion of TCR sequence overlap between unstimulated and stimulated conditions. The majority of unstimulated cells were neither CMV-specific nor HIV-1-specific cells.

(I) Heatmap indicating the proportion of TCR sequence overlap between unstimulated CD4$^+$ T cells and antigen-specific CD4$^+$ T cells.

(J–L) Genes ranked by correlation with T cell clone size were analyzed by GSEA to determine whether the gene expression profile is enriched in specific immune pathways, such as Goldrath antigen response (J), Hallmark TNF signaling via NF-κB (K), and Bosco Th1 cytotoxic module (L). Representative leading-edge genes are shown in each panel. Thick lines indicate the mean enrichment score for each condition and think lines indicate the enrichment score for each individual. See also Figures S3 and S4.

Please cite this article in press as: Collora et al., Single-cell multiomics reveals persistence of HIV-1 in expanded cytotoxic T cell clones, Immunity (2022), https://doi.org/10.1016/j.immuni.2022.03.004

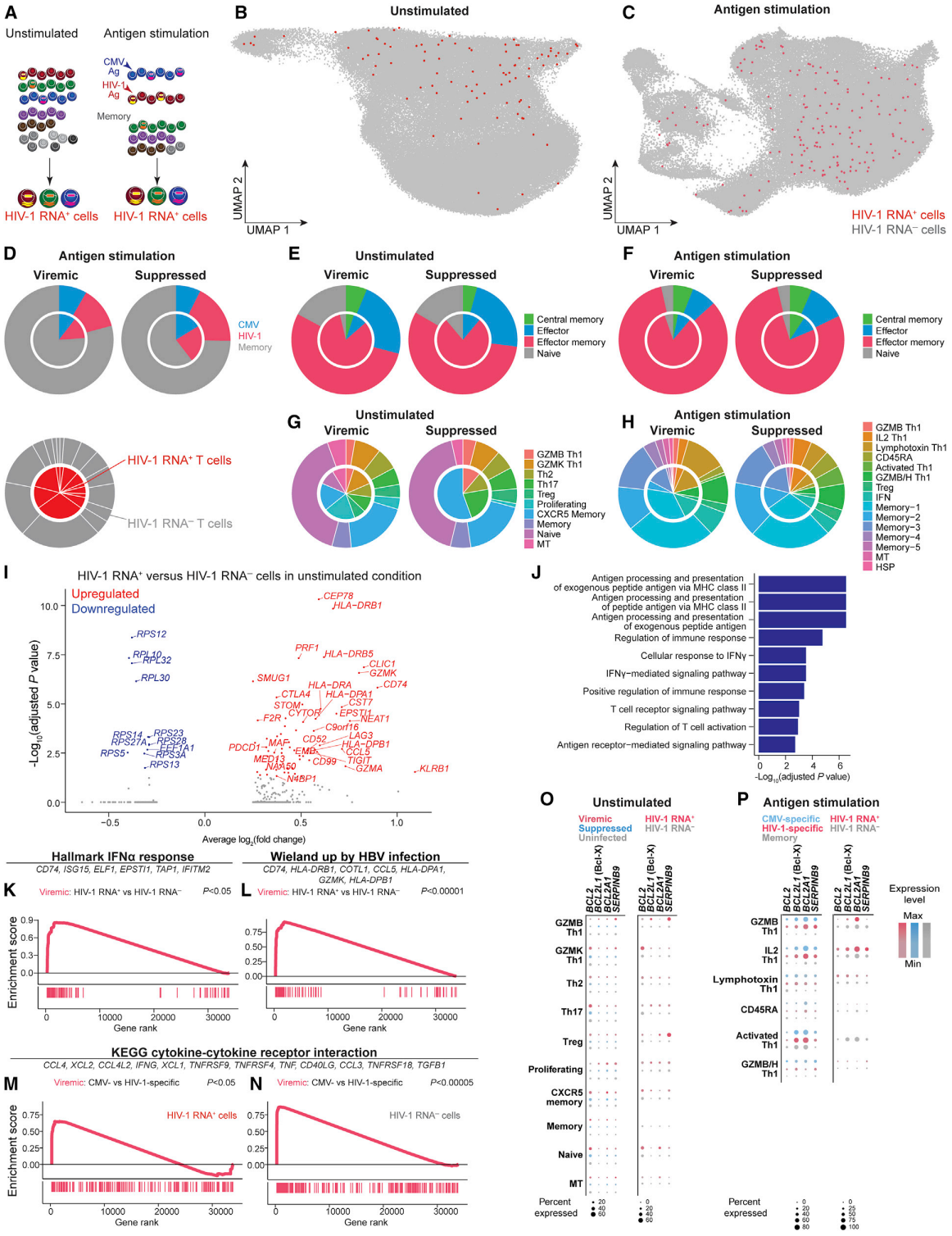

(legend on next page)

Please cite this article in press as: Collora et al., Single-cell multiomics reveals persistence of HIV-1 in expanded cytotoxic T cell clones, Immunity (2022), https://doi.org/10.1016/j.immuni.2022.03.004

in CMV-specific and HIV-1-specific cells, there was no enrichment or proportional differences of HIV-1-RNA$^+$ cells in CMV-specific or HIV-1-specific cells (Wilcoxon rank-sum test).

When we examined the distribution of HIV-1 RNA$^+$ cells in memory cell subsets, we found that HIV-1 RNA$^+$ cells were enriched in effector memory in unstimulated viremic ($p < 2.2 \times 10^{-16}$, Fisher's exact test) conditions (Figure 4E) but not in stimulated conditions (Figure 4F), generally consistent with previous studies of HIV-1 enrichment in effector memory cells (Cole et al., 2021; Duette et al., 2022; Hiener et al., 2017). When we examined the distribution of HIV-1 RNA$^+$ cells in transcriptome defined clusters, HIV-1 RNA$^+$ cells were identified from 9 out 10 different clusters in the unstimulated condition, highlighting the heterogeneity of HIV-1 RNA$^+$ cells *in vivo*. By comparing the proportion of HIV-1 RNA$^+$ cells and HIV-1 RNA$^-$ cells in these clusters, we found that there was enrichment of HIV-1 RNA$^+$ cells during viremia in GZMK Th1 ($p = 0.049$) and proliferating cells ($p = 0.00000001$) and dis-enrichment of HIV-1 RNA$^+$ cells in naive cells ($p = 0.00006$) and non-polarized memory cells ($p = 0.02$) in the unstimulated condition (Figure 4G). In antigen-stimulated conditions, HIV-1 RNA$^+$ cells were identified from 14 out of 15 different clusters. We found that there was no enrichment of HIV-1 RNA$^+$ cells in specific clusters and there was dis-enrichment of HIV-1 RNA$^+$ cells in non-polarized IFN ($p = 0.009$) and memory-1 ($p = 0.0001$) clusters (Figure 4H). Because of their limited number, we avoided statistical analysis of HIV-1 RNA$^+$ cells during viral suppression. Overall, we found that HIV-1 RNA$^+$ cells were heterogeneous.

Antigen, IFN, and cytotoxic T cell response shapes the transcriptional landscape of HIV-1 RNA$^+$ cells during viremia

We compared the transcriptional landscape of HIV-1 RNA$^+$ cells versus HIV-1 RNA$^-$ cells only during viremia, as the 9 cells captured during viral suppression were too few for robust analysis. We found that HIV-1 RNA$^+$ cells upregulated cytotoxicity genes (*GZMK*, *GZMA*, *PRF1*, *CEP78*, *CCL5*), major histocompatibility complex (MHC) class II genes (*HLA-DRB1*, *HLA-DPB1*, *CD74*), and exhaustion markers (*PDCD1*, *TIGIT*, *LAG3*, *CTLA4*) (Figure 4I; Table S3). These genes were enriched in antigen presentation and IFN-γ responses (Figure 4J), reflecting antiviral responses during viremia.

To compare the transcriptional landscape of HIV-1 RNA$^+$ cells versus HIV-1 RNA$^-$ cells across different conditions, we ranked genes using expression fold change and conducted gene set enrichment analysis (GSEA) on predefined gene expression signatures. First, when we compared HIV-1 RNA$^+$ cells versus HIV-1 RNA$^-$ cells in unstimulated conditions during viremia, we found that HIV-1 RNA$^+$ cells upregulated IFN-α response (Figure 4K) and viral infection response genes (Figure 4L) ($p < 0.05$), reflecting innate immune responses to acute viral infections. When we compared CMV-specific cells versus HIV-1-specific cells during viremia, we found that CMV-specific cells upregulated cytokine and cytokine receptor genes, both in HIV-1 RNA$^+$ cells (Figure 4M) and HIV-1 RNA$^-$ cells (Figure 4N). This suggests that CMV-specific cells have more robust cytokine responses upon antigen stimulation compared with HIV-1-specific cells.

GZMB Th1 cells express genes encoding anti-apoptotic protein Bcl-xL and cytotoxic CD8$^+$ T cell resistant gene Serpin B9

We wanted to understand why HIV-1 RNA$^+$ cells survived despite HIV-1 expression. Previous studies suggest that Bcl-2 family proteins may promote the survial of HIV-1-infected cells (Ren et al., 2020). We examined the expression levels of the anti-apoptotic *BCL2* (encoding Bcl-2), *BCL2L1* (encoding Bcl-xL), and *BCL2A1* (an nuclear factor κB [NF-κB] target gene upregulated by TNF that promotes cell survival; Vogler, 2012). In unstimulated CD4$^+$ T cells, we found that *BCL2* expression was not significantly different between CD4$^+$ T cells from viremic, suppressed, and uninfected individuals (Figure 4O). When we examined HIV-1 RNA$^+$ cells in the unstimulated condition, *BCL2L1* (Bcl-xL) expression in Th1 polarized clusters (GZMB Th1, Th2, Th17, and proliferating cells) trended higher in HIV-1 RNA$^+$ cells than in HIV-1 RNA$^-$ cells, although this did not reach statistical significance (Figure 4O, Wilcoxon rank-sum test). Upon antigen stimulation, antigen responding cells expressed *BCL2*, *BCL2L1*, and *BCL2A1* in Th1 polarized clusters (GZMB Th1, IL2 Th1, and Lymphotoxin Th1) (Figure 4P). When we examined HIV-1 RNA$^+$ cells in the stimulated condition, *BCL2L1* and *BCL2A1* expression was comparable with that in HIV-1 RNA$^-$ cells.

In addition to Bcl2-family genes, we examined *SERPINB9* gene expression. Granzyme-secreting immune effectors such as cytotoxic CD8$^+$ T cells and natural killer cells express serpin

Figure 4. The heterogeneous transcriptional landscape of HIV-1 RNA$^+$ cells demonstrated antigen responses, cytokine responses, and anti-apoptotic programs

(A) Cells expressing HIV-1 RNA were identified by mapping reads to autologous HIV-1 sequences in addition to HXB2 reference sequence in unstimulated conditions and stimulated conditions (including CMV-specific, and HIV-specific, and memory cells). HIV-1 RNA$^+$ cells were defined by having at least 2 HIV-1-related UMI or at least 4 reads of a single UMI to guard against index hopping and sequencing artifacts.

(B and C) UMAP plots showing HIV-1 RNA$^+$ cells in unstimulated (B), antigen-specific, and memory cells (C).

(D–H) Pie charts indicating the distribution of antigen specificity (D), memory phenotype in unstimulated (E) and in antigen stimulated conditions (F), and transcriptionally defined clusters in unstimulated conditions (G) and in antigen stimulated conditions (H). The inner chart represents HIV-1 RNA$^+$ cells and the outer chart represents HIV-1 RNA$^-$ cells.

(I) Volcano plot indicating differentially expressed genes between HIV-1 RNA$^+$ and HIV-1 RNA$^-$ cells in the unstimulated condition during viremia.

(J) Gene ontology enrichment of immune pathways from upregulated genes.

(K–N) GSEA plots indicating the enrichment of gene sets in specific immune pathways, including IFN-α response (K), viral response (L), cytokine and cytokine receptor interaction (M and N, respectively). Representative leading-edge genes are shown in each panel.

(O and P) Dot plots showing expression of anti-apoptotic Bcl-2 family genes *BCL2* (encoding Bcl-2), *BCL2L1* (encoding Bcl-xL), and *BCL2A1* and the granzyme B inhibitor *SERPINB9* (encoding Serpin B9) in unstimulated (O) and antigen stimulated conditions (P).

See also Figures S5 and S6 and Table S3.

Please cite this article in press as: Collora et al., Single-cell multiomics reveals persistence of HIV-1 in expanded cytotoxic T cell clones, Immunity (2022), https://doi.org/10.1016/j.immuni.2022.03.004

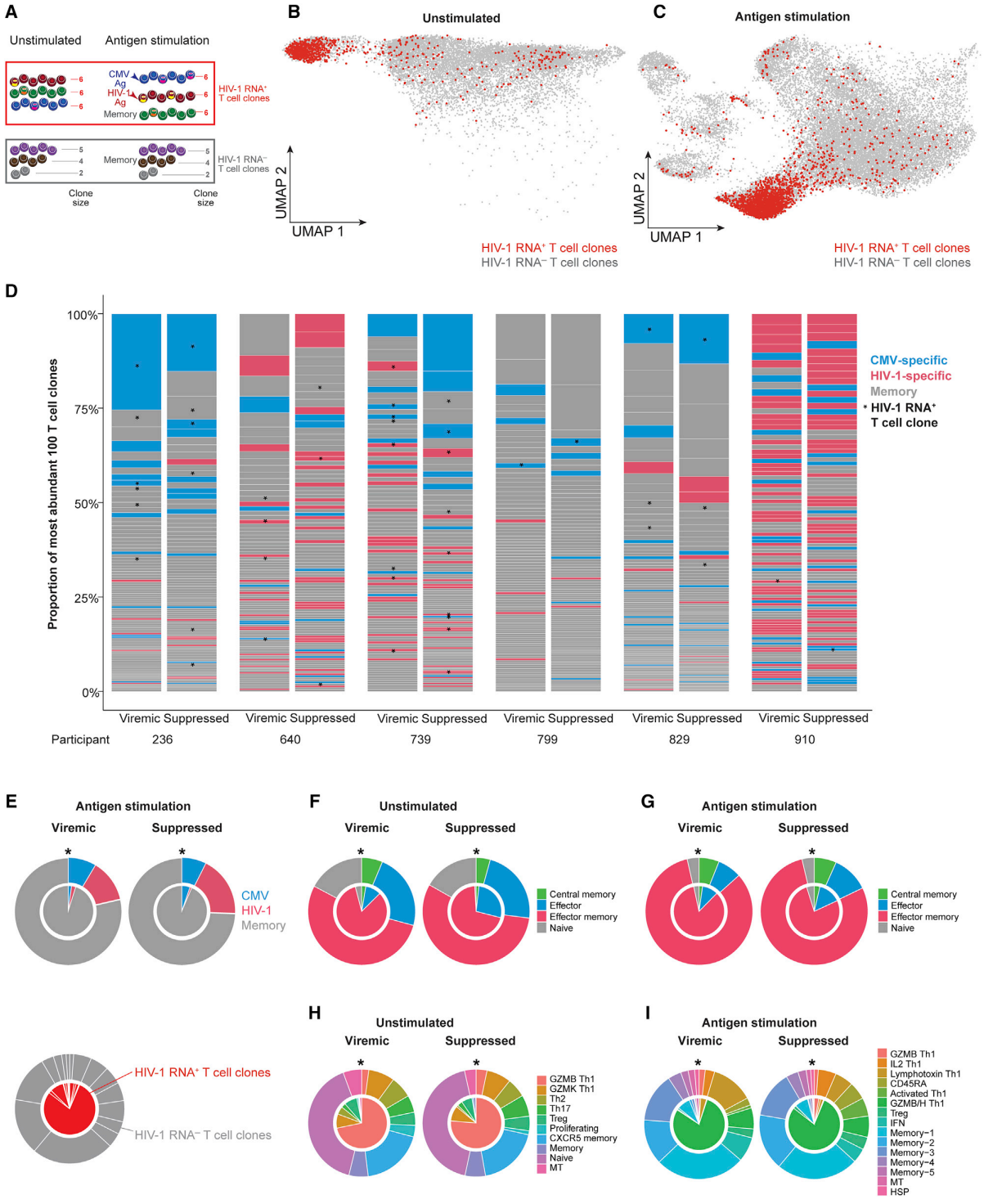

Figure 5. HIV-1 RNA$^+$ T cell clones are enriched in effector memory and GZMB Th1 cells

(A) T cell clones were defined by at least two cells sharing the same TCR sequence. HIV-1 RNA$^+$ T cell clones were defined by T cell clones having at least one HIV-1 RNA$^+$ cells. HIV-1 RNA$^-$ T cell clones were defined by T cell clones not having any HIV-1 RNA$^+$ cells.

(legend continued on next page)

Please cite this article in press as: Collora et al., Single-cell multiomics reveals persistence of HIV-1 in expanded cytotoxic T cell clones, Immunity (2022), https://doi.org/10.1016/j.immuni.2022.03.004

protease inhibitor 9 (Serpin B9) to protect themselves from self-inflicted granule-mediated apoptosis (Bird et al., 1998; Stout-Delgado et al., 2007; Zhang et al., 2006). We reasoned that Serpin B9 expression in cytotoxic CD4$^+$ T cells, while protecting themselves from their own granzyme B-mediated killing, may also make HIV-1-infected cells with a cytotoxic phenotype resistant to cytotoxic CD8$^+$ T cell killing (R. Brad Jones, personal communications). We found that *SERPINB9* expression was higher in HIV-1 RNA$^+$ GZMB Th1 cells in the unstimulated condition, although this trend did not reach statistical significance (Figure 4O). We also found *SERPINB9* expression in GZMB Th1 cells was higher in CMV-specific cells and HIV-1-specific cells than memory cells, but this trend did not reach statistical significance (Figure 4P). Our finding suggests a reason why HIV-1 RNA$^+$ cells may resist cytotoxic CD8$^+$ T cell killing by residing in cytotoxic CD4$^+$ T cells which naturally resist granzyme B-mediated killing through Serpin B9 expression. Given the low number of cells examined, further studies involving more single cell analyses and *in vitro* testing are still required.

The majority of HIV-1 RNA$^+$ T cell clones are GZMB effector memory Th1 cells with unknown antigen specificity but robust antigen responses

We next examined the immune phenotype of T cell clones harboring HIV-1 RNA$^+$ cells (termed HIV-1 RNA$^+$ T cell clones) versus T cell clones not harboring HIV-1 RNA$^+$ cells (termed HIV-1 RNA$^-$ T cell clones). Of note, in an HIV-1 RNA$^+$ T cell clone, only a subset of cells are expressing HIV-1 RNA, while the remaining are uninfected or have latent HIV-1. These are T cells responding to the same antigen (having the same TCR sequence), with one or a few of these T cells within the clone having detectable HIV-1 RNA$^+$ (Figure 5A). Unlike the heterogeneity of HIV-1 RNA$^+$ T cells, HIV-1 RNA$^+$ T cell clones were enriched in specific clusters, mainly GZMB Th1 cells in unstimulated samples (Figure 5B) and in GZMB/H Th1 cells in the antigen-stimulated condition (Figure 5C). When we examined the antigen specificity of the largest 100 T cell clones in each individual, we found that CMV-specific and HIV-1-specific T cell clones were frequently captured in these 100 largest clones (Figure 5D). We found that significantly more HIV-1 RNA$^+$ T cell clones were memory T cells that did not respond to CMV and HIV-1 antigen stimulation (Fisher's exact test, $p < 0.001$, both viremia and viral suppression), and there was no enrichment of HIV-1 RNA$^+$ T cell clones in CMV or HIV-1-specific cells (Figure 5E). When we examined the memory cell phenotype, we found that more HIV-1 RNA$^+$ T cell clones were in enriched in effector memory cells relative to HIV-1 RNA$^-$ T cell clones in unstimulated ($p < 0.001$, both viremia and viral suppression) but not stimulated conditions (Figures 5F and 5G). When we examined the transcriptome-defined cell clusters, we found that cells in HIV-1 RNA$^+$ T cell clones were enriched in the GZMB Th1 cluster in unstimulated conditions (Figure 5H, $p < 0.001$, both viremia and viral suppression) and the GZMB/H Th1 cluster in stimulated conditions (Figure 5I, $p < 0.001$, both viremia and viral suppression). We found that within single T cell clones, there were limited transcriptional, cluster, or memory phenotype changes between viremia and after viral suppression (Table S4; Figures S6A–S6F). Our results indicate that HIV-1 takes the advantage of the immune system by infecting and persisting in *GZMB*$^+$ effector memory T cell clones that are hardwired with strong antigen responses and robust clonal expansion capacity.

HIV-1 RNA$^+$ T cell clones, mainly GZMB Th1, are larger in clone size, stable, and persist over time

We examined the T cell clone size and clonal expansion dynamics of HIV-1 RNA$^+$ T cell clones over time, during viremia and after viral suppression. We found that HIV-1 RNA$^+$ T cell clones were significantly larger in clone size than HIV-1 RNA$^-$ T cell clones both during viremia and after viral suppression, in unstimulated CD4$^+$ T cells (Figure 6A) and after antigen stimulation in CMV-specific cells (Figure 6B), HIV-1-specific cells (Figure 6C), and memory cells (Figure 6D). The enrichment of HIV-1 in larger T cell clones may be because larger T cell clones are more likely to be infected or detected by chance. To test this possibility, we conducted a permutation-based approach. We found that in HIV-1 and CMV-specific T cell clones, both during viremia and viral suppression (Figures S6G–S6N), the permutation test did not reach statistical significance. This result suggests that HIV-1-specific or CMV-specific T cell clones were larger in size and therefore more likely to harbor HIV-1 RNA$^+$ cells by chance. After viral suppression, these large HIV-1-specific or CMV-specific T cell clones were maintained at larger clone size because of chronic antigen stimulation or robust proliferation. In contrast, in memory cells and in unstimulated conditions, HIV-1 RNA$^+$ T cell clones were larger than HIV-1 RNA$^-$ T cell clones (significantly larger than all 10,000 permutations, Wilcoxon rank-sum test). This result suggests that HIV-1 RNA$^+$ T cell clones (with unknown antigen specificity) have preferential survival or proliferation over HIV-1 RNA$^-$ T cell clones.

We next examined T cell clonal expansion dynamics by measuring the fold change of T cell clone size between viremia and viral suppression. We found that the majority of HIV-1 RNA$^+$ T cell clones remained stable (at the same clone size) between viremia and viral suppression, particularly HIV-1-specific cells and CMV-specific cells (Figure 6E). HIV-1 RNA$^-$ T cell clones had a greater diversity of fold changes in T cell clone size (Figure 6E). To measure T cell clone persistence, we counted T cell clones that were captured both during viremia and after viral suppression versus those that were captured at only one time point. We found that HIV-1 RNA$^+$ clones were more persistent in both unstimulated and stimulated conditions in CMV-specific cells, HIV-1-specific cells, and memory cells (Figure 6F). When we examined the immune phenotype of T cell clones that persisted over time, we found that they were GZMB Th1 cells in the unstimulated condition (Figures 6G and 6H) and GZMB/H Th1 cells in the antigen stimulated condition

(B and C) UMAP plots indicating HIV-1 RNA$^+$ T cell clone in unstimulated (B) and antigen stimulated conditions (C).
(D) The largest 100 T cell clones, as measured by bulk TCR sequencing in each participant at each time point. * in D, HIV-1 RNA$^+$ clones.
(E–I) Pie charts indicating the distribution of antigen specificity (E), memory phenotype in unstimulated (F) and in antigen stimulated conditions (G), transcriptionally defined clusters in unstimulated conditions (H) and in antigen stimulated conditions (I). * in (E–I), $p < 0.05$, Fisher's exact test.
See also Figures S5 and S6 and Table S4.

Please cite this article in press as: Collora et al., Single-cell multiomics reveals persistence of HIV-1 in expanded cytotoxic T cell clones, Immunity (2022), https://doi.org/10.1016/j.immuni.2022.03.004

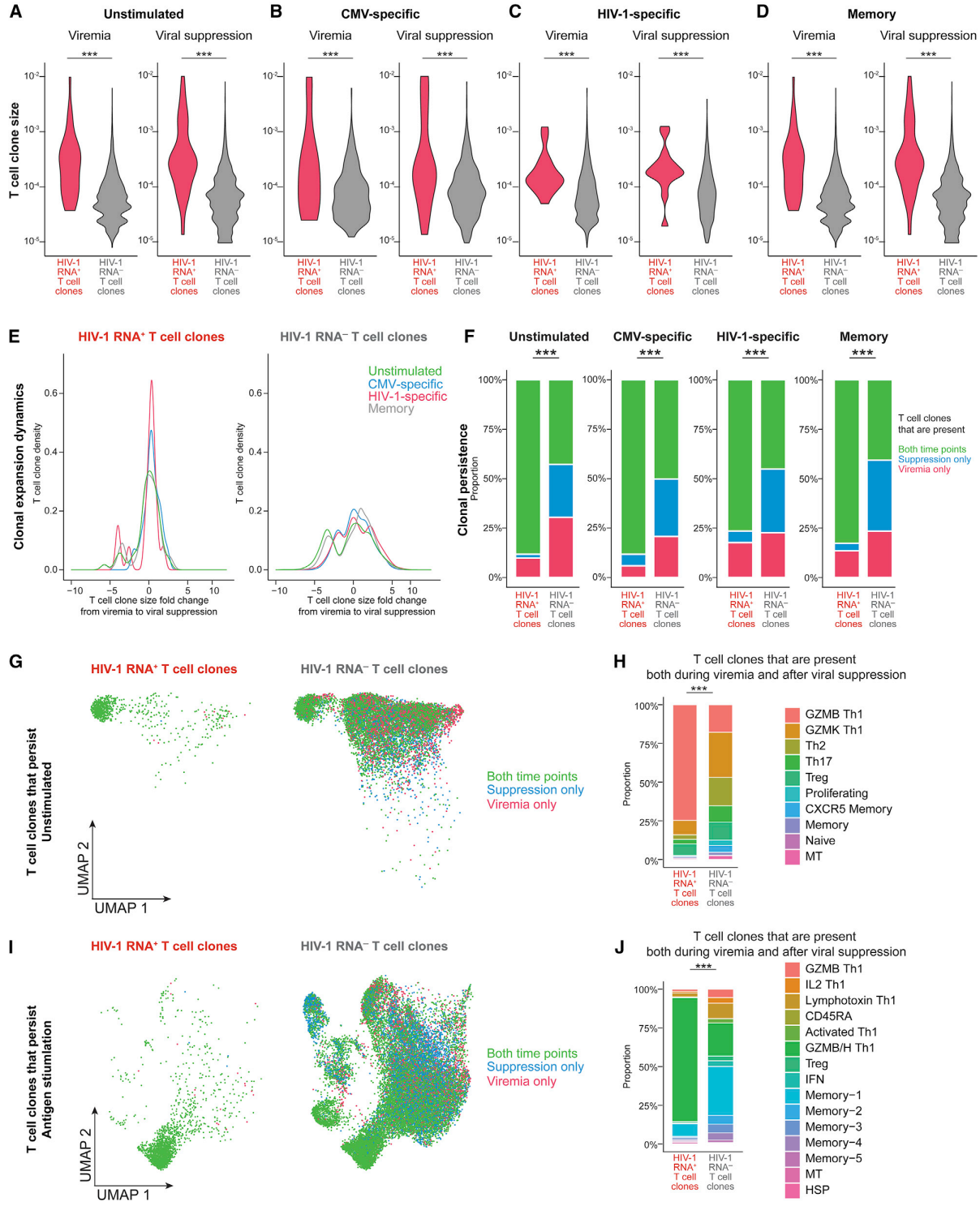

Figure 6. HIV-1 RNA+ T cell clones are large and persistent in GZMB and GZMB/H Th1 cells

(A–D) T cell clone size, as measured by the frequency of T cells sharing the same TCR sequence, in unstimulated (A) and antigen stimulated conditions in CMV-specific (B), HIV-1-specific (C), and memory cells (D). p values were determined by the Wilcoxon rank-sum test.

(E) T cell clonal expansion dynamics, as measured by the fold change of T cell clone size from viremia to viral suppression.

(legend continued on next page)

Please cite this article in press as: Collora et al., Single-cell multiomics reveals persistence of HIV-1 in expanded cytotoxic T cell clones, Immunity (2022), https://doi.org/10.1016/j.immuni.2022.03.004

(Figures 6I and 6J). Overall, we found that HIV-1 RNA$^+$ T cell clones are larger in clone size, stable, and persistent over time.

HIV-1 RNA$^+$ T cell clones upregulate cytotoxic T cell genes

We next wanted to identify transcriptional differences between HIV-1 RNA$^+$ versus HIV-1 RNA$^-$ T cell clones. Using GSEA, we found that HIV-1 RNA$^+$ T cell clones upregulated cytotoxic T cell genes (such as *GZMB*, *GZMH*, *GZMA*, *PFN1*, *CCL5*, *CST7*, *NKG7*) and *IL2RG* (Figures 7A and 7B). To identify predictors that can differentiate HIV-1 RNA$^+$ T cell clones from HIV-1 RNA$^-$ T cell clones, we used the machine-learning tool single-cell identity definition using random forests and recursive feature elimination (scRFE) to identify a subset of genes that were necessary and sufficient to differentiate HIV-1 RNA$^+$ from HIV-1 RNA$^-$ T cell clones. We completed scRFE with 10,000 replicates and selected the top 200 genes which maximized model specificity and sensitivity (Figures S7A–S7C; Table S4). These 200 genes included both differentially expressed genes and nondifferentially expressed genes, highlighting this model's ability to identify key genes that define populations beyond simple differential gene expression (Figure 7C). Upregulated genes identified by scRFE were enriched for pathways related to IFN responses, viral infection, IL-12 signaling, and T cell signaling (Figure 7D).

A significantly higher proportion of HIV-1 p24 effector memory CD4$^+$ T cells are granzyme B positive

To validate our findings, we tested whether granzyme B$^+$ effector memory cells were enriched for HIV-1-infected cells. Using flow cytometry, we examined granzyme B protein expression in HIV-1-infected cells that expressed p24 protein upon phorbol myristate acetate (PMA)/ionomycin activation (Figure 7E; Figure S7C). We first used CD4$^+$ T cells from the Sabes cohort during viremia and after viral suppression. We found that in effector memory cells, HIV-1 p24$^+$ cells are granzyme B$^+$ particularly during viral suppression (Figure 7F). CTLA4, a cellular marker known to enrich for HIV-1 RNA$^+$ cells (Figure 4I) (McGary et al., 2017), was enriched in HIV-1 p24$^+$ cells in the Sabes cohort, both during viremia and viral suppression (Figure 7G). We examined other Th1 effector proteins such as IFN-γ and TNF expression to examine whether HIV-1 p24$^+$ cells were simply enriched in polarized Th1 cells. We found that IFN-γ and TNF expressing cells were not enriched in HIV-1 p24$^+$ cells (Figures 7H and 7I).

To examine whether the enrichment of HIV-1 p24$^+$ cells in granzyme B$^+$ population is generalizable to other infected individuals, we recruited study participants from a separate cohort from the Wistar Institute. Study participants recruited at the Wistar cohort had a longer duration of undetectable viral load (mean 75 months in the Wistar cohort versus 8 months in the Sabes cohort, $p = 0.006$, two-tailed Student's t test), different ages (mean 44.1 years versus 24.5 years, $p = 0.0004$), different ethnicity (non-Hispanic versus Hispanic) from different geographic locations (Philadelphia versus Lima). We found that granzyme B$^+$ effector memory T cells were enriched in HIV-1 p24$^+$ cells compared with HIV-1 p24$^-$ cells (Figure 7J), while CTLA4, IFN-γ, and TNF expression were not significantly enriched in HIV-1 p24$^+$ cells (Figures 7K, 7L, and 7M). Overall, we found that *GZMB*$^+$ cytotoxic effector memory CD4$^+$ T cells were enriched for inducible HIV-1-infected cells.

DISCUSSION

HIV-1 persists in proliferating CD4$^+$ T cells despite suppressive ART. To reach a cure, key questions need to be answered: which cell subsets harbor HIV-1, what drives the proliferation and persistence of HIV-1-infected cells, and how do HIV-1-infected cells resist cell death despite HIV-1 reactivation? By combining single-cell profiling methods, bioinformatic analysis, and machine-learning algorithms on longitudinally archived blood samples from the prospective Sabes study, we tracked HIV-1 RNA$^+$ T cell clones from viremia to viral suppression. We found that antigen responses and TNF responses persisted despite suppressive ART, indicating ongoing antigen stimulation from existing HIV-1-infected cells and other co-infections as a cause of chronic immune activation. Antigen, TNF, and cytotoxic T cell responses determined T cell clone size. By comparing cells sharing the same TCR between unstimulated conditions and after antigen stimulation, we found that CMV-specific cells were primed as GZMB Th1 in unstimulated conditions, while HIV-1-specific cells were primed as Th17 and proliferating cells in unstimulated conditions. We identified HIV-1 RNA$^+$ cells without *ex vivo* stimulation and found that HIV-1 RNA$^+$ cells were heterogeneous, that no single marker could exclusively distinguish HIV-1 RNA$^+$ cells from HIV-1 RNA$^-$ cells. By tracking T cell clonal expansion dynamics—namely T cell clone size, stability, persistence, and transcriptional phenotype—both in unstimulated conditions (reflecting the *in vivo* status of the cells) and after CMV and HIV-1 antigen stimulation (reflecting antigen responses), we found that HIV-1 RNA$^+$ T cell clones had unique signatures as cytotoxic effector memory CD4$^+$ T cells expressing granzyme B. Using machine-learning algorithms, we identified key genes that could distinguish HIV-1 RNA$^+$ T cell clones from HIV-1 RNA$^-$ T cell clones. By testing our transcriptome-based findings with protein-based validations using flow cytometry, both from the Sabes study and an independent Wistar cohort, we validated our result and confirmed that HIV-1-infected cells resided in granzyme B$^+$ Th1 effector memory CD4$^+$ T cells after suppressive ART. It is plausible that these cells resist cell death by Bcl-2 family gene expression and are shielded from cytotoxic CD8$^+$ T cell killing because of Serpin B9 expression, but further studies are needed to test this possibility. Our study indicates that HIV-1 persists by residing in cells having robust antigen responses, proliferation potential, and long-term clonal stability.

(F) T cell clonal persistence, as measured by the proportion of T cell clones that can be captured both during viremia and after viral suppression versus those that can be captured at one time point.
(G and I) UMAP plots showing T cell clones that persisted both during viremia and after viral suppression in unstimulated (G) and antigen-stimulated conditions (I).
(H and J) The proportion of transcriptionally defined T cell clusters in T cell clones that persisted both during viremia and after viral suppression in unstimulated (H) and antigen-stimulated (J) conditions.
In F, H, and J, p values were determined by Fisher's exact test. ***$p < 0.001$. See also Figure S6.

Please cite this article in press as: Collora et al., Single-cell multiomics reveals persistence of HIV-1 in expanded cytotoxic T cell clones, Immunity (2022), https://doi.org/10.1016/j.immuni.2022.03.004

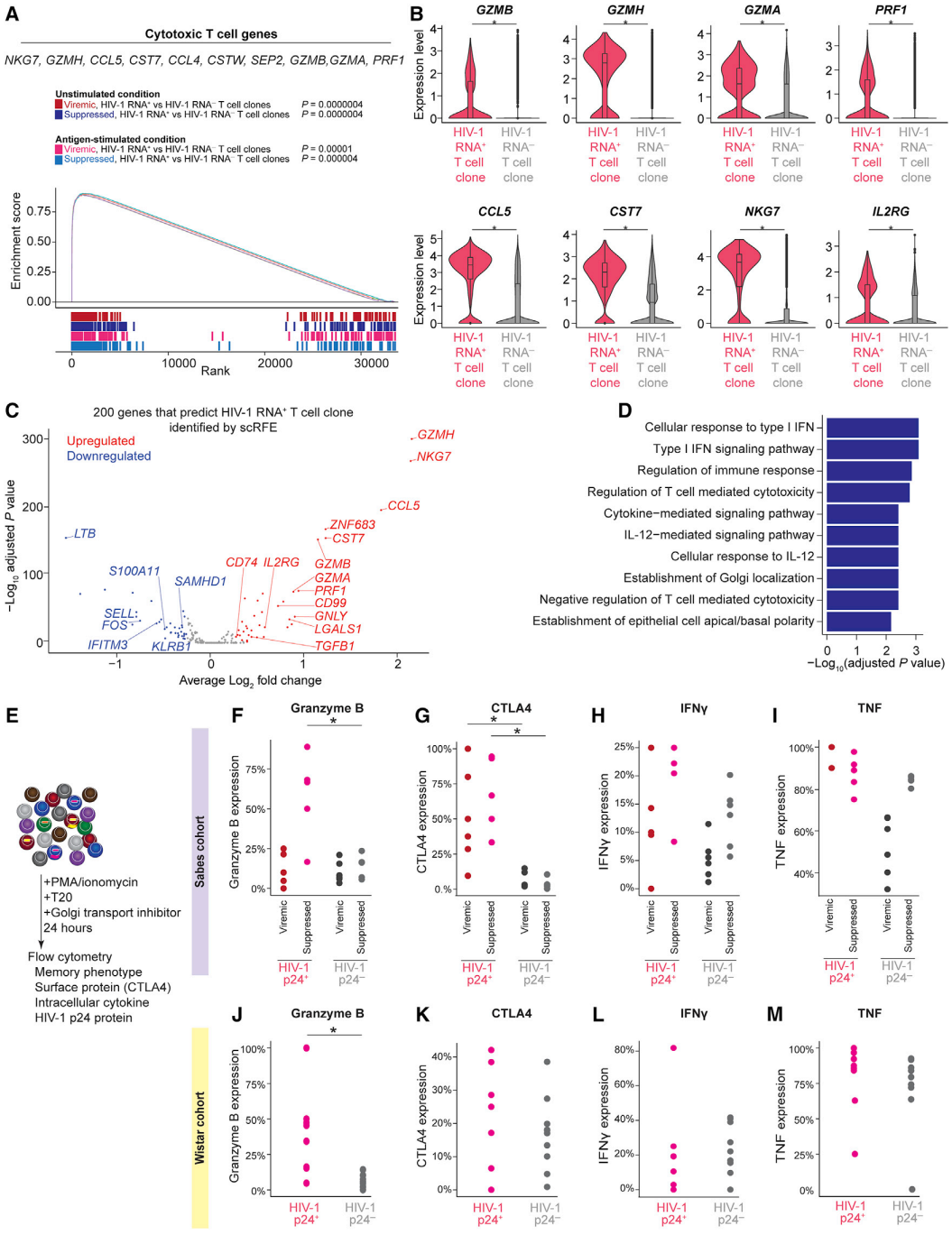

Figure 7. HIV-1 RNA$^+$ T cell clones are enriched in effector memory CD4$^+$ T cells and express cytotoxic T cell genes

(A) GSEA plot and example leading-edge genes (the top genes enriched in this pathway) showing enrichment of gene expression in T cell activation genes (GSE45739 unstimulated versus anti-CD3/CD28 stimulated CD4 T cell upregulated) in HIV-1 RNA$^+$ T cell clones.

(B) Expression level of cytotoxic T cell response genes. p values were derived from Wilcoxon rank-sum test. (C) The 200 genes necessary and sufficient to differentiate HIV-1 RNA$^+$ T cell clone from HIV-1 RNA$^-$ T cell clone were identified using single-cell identity definition using random forests and recursive feature elimination (scRFE). The volcano plot showed differential expression of the 200 scRFE defined genes. p values were derived from Wilcoxon rank-sum test.

(D) Enriched immune pathways of upregulated genes among the 200 genes necessary and sufficient to differentiate HIV-1 RNA$^+$ T cell clone from HIV-1 RNA$^-$ T cell clones. p values were calculated by Fisher's exact test.

(legend continued on next page)

Please cite this article in press as: Collora et al., Single-cell multiomics reveals persistence of HIV-1 in expanded cytotoxic T cell clones, Immunity (2022), https://doi.org/10.1016/j.immuni.2022.03.004

The maintenance of these HIV-1 RNA$^+$ T cell clones can be further fueled by HIV-1-induced chronic immune activation through TNF signaling.

The dose and duration of antigen stimulation determines the activation, proliferation capacity, and fate of T cells (Iezzi et al., 1998). We found that CMV-specific cells were highly polarized *GZMB*$^+$ cytotoxic CD4$^+$ T cells while HIV-1-specific cells, likely responding to heterogeneous HIV-1 antigen stimulation, were polarized into different effector phenotypes but were not able to polarize into *GZMB*$^+$ cytotoxic T cells. Further, different memory T cells may have different proliferation rate: the estimated proliferation rate is highest in effector memory CD4$^+$ T cells (0.042/day), followed by central memory CD4$^+$ T cells (0.01/day) and naive CD4$^+$ T cells (0.004/day) (Macallan et al., 2019). Our finding suggests that by residing in T cells that have robust proliferative capacity, such as cytotoxic effector memory CD4$^+$ T cells, the clonally expanding HIV-1-infected cells can be maintained by chronic antigen stimulation. Although CMV-specific and HIV-1-specific CD4$^+$ T cells only account for a small proportion of antigen-specific cells, eliminating immune drivers of clonal expansion, such as by controlling CMV infection (Hunt et al., 2011), inhibiting HIV-1 expression (Yeh et al., 2020), and reducing TNF-induced chronic immune activation, may halt the clonal expansion of HIV-1-infected cells and accelerate HIV-1 eradication.

Limitations of the study

A major limitation of this study is that this method does not capture HIV-1 latently infected cells that do not express HIV-1 RNA. Methods that can capture HIV-1 DNA, HIV-1 RNA, and cellular transcriptome within the same cell are needed to examine the immune profile of the transcriptionally silent latently infected cells, which can potentially be achieved by advanced technologies. Still, recent studies have demonstrated that up to 30% of the HIV-1-infected cells actively express HIV-1 RNA and persist over time despite ART (Einkauf et al., 2022). The result highlights the importance of understanding both transcriptionally active and latent HIV-1-infected cells.

STAR★METHODS

Detailed methods are provided in the online version of this paper and include the following:

- KEY RESOURCES TABLE
- RESOURCE AVAILABILITY
  - Lead contact
  - Materials availability
  - Data and code availability
- EXPERIMENTAL MODEL AND SUBJECT DETAILS
  - Study participants
- METHOD DETAILS
  - Isolation of unstimulated and antigen-specific CD4$^+$ T cells
  - DNA-barcoded surface protein staining
  - ECCITE-seq library preparation and sequencing
  - Bulk T cell receptor library preparation and sequencing
  - Autologous HIV-1 sequencing
  - Flow cytometric validation
  - Single-cell multi-omic analysis
  - Permutation testing of observed HIV-1 RNA$^+$ clone size relative to overall clone size distribution
  - Elastic net clonal regression
  - Single-cell recursive feature elimination and random forest validation (scRFE)
  - Pathway enrichment analysis
- QUANTIFICATION AND STATISTICAL ANALYSIS

SUPPLEMENTAL INFORMATION

Supplemental information can be found online at https://doi.org/10.1016/j.immuni.2022.03.004.

ACKNOWLEDGMENTS

We thank all study participants. We thank Alex Shalek, Sam Kazer, Carly Ziegler, Joseph Craft, Steven Kleinstein, Roy Jiang, Nicolas Chomont, Pierre Gantner, Michael Betts, Vincent Wu, Dan Kaufmann, Elsa Brunet-Ratnasingham, and R. Brad Jones for their insightful suggestions. We thank Siavash Pasalar, Beth Peterson, and Kenneth Lynn for coordinating study participant recruitment. This work is supported by Yale Top Scholar, Rudolf J. Anderson Fellowship, NIH R01 AI141009, NIH R61/R33 DA047037, NIH R37 AI147868, NIH R01 DA051906, NIH R01AI145164, NIH UM1 DA051410, NIH U01 DA053628, NIH CHEETAH P50 AI150464, NIH REACH Martin Delaney Collaboratory UM1 AI164565, NIH BEAT-HIV Martin Delaney Collaboratory UM1 AI126620, Gilead HIV Research Scholar, and American Foundation for AIDS Research (amfAR 110029-67-RGRL) (Y.-C.H and D.D.); NIH R35 GM143072 (D.D.); the Robert I. Jacobs Fund of The Philadelphia Foundation (L.J.M.); Yale Gruber Fellowship (J.A.C.); NIH T32 AI055403 (J.A.C.); and a Yale Center for Genome Analysis-10X Genomics Pilot Award (R.L). The Sabes and MERLIN studies were supported by NIH R01 DA032106 and NIH R01 DA040532 (A.D.). We thank NIH HIV Reagent Program providing antigen peptides and enfuvirtide. We gratefully acknowledge ART drug donation from Merck & Co. and Gilead Sciences Inc for the Sabes and Merlin cohorts.

AUTHOR CONTRIBUTIONS

J.A.C., R.L., and Y.-C.H. designed the experiments, performed analyses, and wrote the manuscript. J.A.C. and R.L. performed experiments. J.A.C. led bioinformatic analyses and R.L. contributed. J.A.C. performed machine-learning analyses with help from N.R. and D.v.D. D.P.-S., C.G., R.A., J.R.L., J.C., S.S., K.M., P.T., L.J.M., and A.D. recruited study participants and processed clinical samples. A.D. designed the Sabes and MERLIN studies and assumed oversight for study conduct and analysis.

DECLARATION OF INTERESTS

The authors declare no competing interests.

(E) To validate the enrichment of HIV-1 RNA$^+$ cells in *GZMB*$^+$, *CTLA4*$^+$, and effector memory populations at the protein level, we stimulated CD4$^+$ T cells with PMA and ionomycin in the presence of ART (T20) and Golgi transport inhibitors for 24 h.

(F–M) We then measured HIV-1 p24 protein expression, memory markers, granzyme B, CTLA4, IFN-γ, and TNF protein expression in the Sabes cohort (F–I) and the Wistar cohort (J–M). Study participants in these two cohorts were significantly different in the duration of viral suppression, age, ethnicity, and geographic locations. p values were derived from Wilcoxon rank-sum test.

*$p < 0.05$; ***$p < 0.001$. See also Figure S7 and Table S4.

Please cite this article in press as: Collora et al., Single-cell multiomics reveals persistence of HIV-1 in expanded cytotoxic T cell clones, Immunity (2022), https://doi.org/10.1016/j.immuni.2022.03.004

CellPress

INCLUSION AND DIVERSITY

One or more of the authors of this paper self-identifies as living with a disability. One or more of the authors of this paper self-identifies as an underrepresented ethnic minority in science. One or more of the authors of this paper received support from a program designed to increase minority representation in science.

Received: October 25, 2021
Revised: February 19, 2022
Accepted: March 8, 2022
Published: March 22, 2022

REFERENCES

Appay, V., Zaunders, J.J., Papagno, L., Sutton, J., Jaramillo, A., Waters, A., Easterbrook, P., Grey, P., Smith, D., McMichael, A.J., et al. (2002). Characterization of CD4(+) CTLs ex vivo. J. Immunol. *168*, 5954–5958.

Bailey, J.R., Sedaghat, A.R., Kieffer, T., Brennan, T., Lee, P.K., Wind-Rotolo, M., Haggerty, C.M., Kamireddi, A.R., Liu, Y., Lee, J., et al. (2006). Residual human immunodeficiency virus type 1 viremia in some patients on antiretroviral therapy is dominated by a small number of invariant clones rarely found in circulating CD4+ T cells. J. Virol. *80*, 6441–6457.

Barreiro, L.B., and Quintana-Murci, L. (2010). From evolutionary genetics to human immunology: how selection shapes host defence genes. Nat. Rev. Genet. *11*, 17–30.

Becht, E., McInnes, L., Healy, J., Dutertre, C.-A., Kwok, I.W.H., Ng, L.G., Ginhoux, F., and Newell, E.W. (2018). Dimensionality reduction for visualizing single-cell data using UMAP. Nat. Biotechnol. *37*, 38.

Bengsch, B., Ohtani, T., Khan, O., Setty, M., Manne, S., O'Brien, S., Gherardini, P.F., Herati, R.S., Huang, A.C., Chang, K.-M., et al. (2018). Epigenomic-Guided Mass Cytometry Profiling Reveals Disease-Specific Features of Exhausted CD8 T Cells. Immunity *48*, 1029–1045.e5.

Benjamini, Y., and Hochberg, Y. (1995). Controlling the False Discovery Rate - a Practical and Powerful Approach to Multiple Testing. J. R. Stat. Soc. Series B Stat. Methodol. *57*, 289–300.

Bird, C.H., Sutton, V.R., Sun, J., Hirst, C.E., Novak, A., Kumar, S., Trapani, J.A., and Bird, P.I. (1998). Selective regulation of apoptosis: the cytotoxic lymphocyte serpin proteinase inhibitor 9 protects against granzyme B-mediated apoptosis without perturbing the Fas cell death pathway. Mol. Cell. Biol. *18*, 6387–6398.

Bosque, A., Famiglietti, M., Weyrich, A.S., Goulston, C., and Planelles, V. (2011). Homeostatic proliferation fails to efficiently reactivate HIV-1 latently infected central memory CD4+ T cells. PLoS Pathog. *7*, e1002288.

Brown, D.M., Lee, S., Garcia-Hernandez, Mde.L., and Swain, S.L. (2012). Multifunctional CD4 cells expressing gamma interferon and perforin mediate protection against lethal influenza virus infection. J. Virol. *86*, 6792–6803.

Bruner, K.M., Murray, A.J., Pollack, R.A., Soliman, M.G., Laskey, S.B., Capoferri, A.A., Lai, J., Strain, M.C., Lada, S.M., Hoh, R., et al. (2016). Defective proviruses rapidly accumulate during acute HIV-1 infection. Nat. Med. *22*, 1043–1049.

Bruner, K.M., Wang, Z., Simonetti, F.R., Bender, A.M., Kwon, K.J., Sengupta, S., Fray, E.J., Beg, S.A., Antar, A.A.R., Jenike, K.M., et al. (2019). A quantitative approach for measuring the reservoir of latent HIV-1 proviruses. Nature *566*, 120–125.

Bui, J.K., Sobolewski, M.D., Keele, B.F., Spindler, J., Musick, A., Wiegand, A., Luke, B.T., Shao, W., Hughes, S.H., Coffin, J.M., et al. (2017). Proviruses with identical sequences comprise a large fraction of the replication-competent HIV reservoir. PLoS Pathog. *13*, e1006283.

Chawla, N.V., Bowyer, K.W., Hall, L.O., and Kegelmeyer, W.P. (2002). SMOTE: Synthetic Minority Over-sampling Technique. J. Artif. Intell. Res. *16*, 321–357.

Chen, E.Y., Tan, C.M., Kou, Y., Duan, Q., Wang, Z., Meirelles, G.V., Clark, N.R., and Ma'ayan, A. (2013). Enrichr: interactive and collaborative HTML5 gene list enrichment analysis tool. BMC Bioinformatics *14*, 128.

Chomont, N., El-Far, M., Ancuta, P., Trautmann, L., Procopio, F.A., Yassine-Diab, B., Boucher, G., Boulassel, M.R., Ghattas, G., Brenchley, J.M., et al. (2009). HIV reservoir size and persistence are driven by T cell survival and homeostatic proliferation. Nat. Med. *15*, 893–900.

Chun, T.W., Stuyver, L., Mizell, S.B., Ehler, L.A., Mican, J.A., Baseler, M., Lloyd, A.L., Nowak, M.A., and Fauci, A.S. (1997). Presence of an inducible HIV-1 latent reservoir during highly active antiretroviral therapy. Proc. Natl. Acad. Sci. USA *94*, 13193–13197.

Coffin, J.M., Wells, D.W., Zerbato, J.M., Kuruc, J.D., Guo, S., Luke, B.T., Eron, J.J., Bale, M., Spindler, J., Simonetti, F.R., et al. (2019). Clones of infected cells arise early in HIV-infected individuals. JCI Insight *4*, e128432.

Cohn, L.B., da Silva, I.T., Valieris, R., Huang, A.S., Lorenzi, J.C.C., Cohen, Y.Z., Pai, J.A., Butler, A.L., Caskey, M., Jankovic, M., and Nussenzweig, M.C. (2018). Clonal $CD4^+$ T cells in the HIV-1 latent reservoir display a distinct gene profile upon reactivation. Nat. Med. *24*, 604–609.

Cole, B., Lambrechts, L., Gantner, P., Noppe, Y., Bonine, N., Witkowski, W., Chen, L., Palmer, S., Mullins, J.I., Chomont, N., et al. (2021). In-depth single-cell analysis of translation-competent HIV-1 reservoirs identifies cellular sources of plasma viremia. Nat. Commun. *12*, 3727.

Crooks, A.M., Bateson, R., Cope, A.B., Dahl, N.P., Griggs, M.K., Kuruc, J.D., Gay, C.L., Eron, J.J., Margolis, D.M., Bosch, R.J., and Archin, N.M. (2015). Precise Quantitation of the Latent HIV-1 Reservoir: Implications for Eradication Strategies. J. Infect. Dis. *212*, 1361–1365.

Dan, J.M., Lindestam Arlehamn, C.S., Weiskopf, D., da Silva Antunes, R., Havenar-Daughton, C., Reiss, S.M., Brigger, M., Bothwell, M., Sette, A., and Crotty, S. (2016). A Cytokine-Independent Approach To Identify Antigen-Specific Human Germinal Center T Follicular Helper Cells and Rare Antigen-Specific CD4+ T Cells in Blood. J. Immunol. *197*, 983–993.

Dobin, A., Davis, C.A., Schlesinger, F., Drenkow, J., Zaleski, C., Jha, S., Batut, P., Chaisson, M., and Gingeras, T.R. (2013). STAR: ultrafast universal RNA-seq aligner. Bioinformatics *29*, 15–21.

Douek, D.C., Brenchley, J.M., Betts, M.R., Ambrozak, D.R., Hill, B.J., Okamoto, Y., Casazza, J.P., Kuruppu, J., Kunstman, K., Wolinsky, S., et al. (2002). HIV preferentially infects HIV-specific CD4+ T cells. Nature *417*, 95–98.

Duette, G., Hiener, B., Morgan, H., Mazur, F.G., Mathivanan, V., Horsburgh, B.A., Fisher, K., Tong, O., Lee, E., Ahn, H., et al. (2022). The HIV-1 proviral landscape reveals Nef contributes to HIV-1 persistence in effector memory CD4+ T-cells. J. Clin. Invest. Published online February 8, 2022. https://doi.org/10.1172/JCI154422.

Einkauf, K.B., Osborn, M.R., Gao, C., Sun, W., Sun, X., Lian, X., Parsons, E.M., Gladkov, G.T., Seiger, K.W., Blackmer, J.E., et al. (2022). Parallel analysis of transcription, integration, and sequence of single HIV-1 proviruses. Cell *185*, 266–282.e15.

Finzi, D., Hermankova, M., Pierson, T., Carruth, L.M., Buck, C., Chaisson, R.E., Quinn, T.C., Chadwick, K., Margolick, J., Brookmeyer, R., et al. (1997). Identification of a reservoir for HIV-1 in patients on highly active antiretroviral therapy. Science *278*, 1295–1300.

Fromentin, R., Bakeman, W., Lawani, M.B., Khoury, G., Hartogensis, W., DaFonseca, S., Killian, M., Epling, L., Hoh, R., Sinclair, E., et al. (2016). CD4+ T Cells Expressing PD-1, TIGIT and LAG-3 Contribute to HIV Persistence during ART. PLoS Pathog. *12*, e1005761.

Gantner, P., Pagliuzza, A., Pardons, M., Ramgopal, M., Routy, J.-P., Fromentin, R., and Chomont, N. (2020). Single-cell TCR sequencing reveals phenotypically diverse clonally expanded cells harboring inducible HIV proviruses during ART. Nat. Commun. *11*, 4089.

Gillet, N.A., Malani, N., Melamed, A., Gormley, N., Carter, R., Bentley, D., Berry, C., Bushman, F.D., Taylor, G.P., and Bangham, C.R. (2011). The host genomic environment of the provirus determines the abundance of HTLV-1-infected T-cell clones. Blood *117*, 3113–3122.

Gupta, N.T., Vander Heiden, J.A., Uduman, M., Gadala-Maria, D., Yaari, G., and Kleinstein, S.H. (2015). Change-O: a toolkit for analyzing large-scale B cell immunoglobulin repertoire sequencing data. Bioinformatics *31*, 3356–3358.

Haghverdi, L., Lun, A.T.L., Morgan, M.D., and Marioni, J.C. (2018). Batch effects in single-cell RNA-sequencing data are corrected by matching mutual nearest neighbors. Nat. Biotechnol. *36*, 421–427.

Please cite this article in press as: Collora et al., Single-cell multiomics reveals persistence of HIV-1 in expanded cytotoxic T cell clones, Immunity (2022), https://doi.org/10.1016/j.immuni.2022.03.004

Halvas, E.K., Joseph, K.W., Brandt, L.D., Guo, S., Sobolewski, M.D., Jacobs, J.L., Tumiotto, C., Bui, J.K., Cyktor, J.C., Keele, B.F., et al. (2020). HIV-1 viremia not suppressible by antiretroviral therapy can originate from large T cell clones producing infectious virus. J. Clin. Invest. *130*, 5847–5857.

Hiener, B., Horsburgh, B.A., Eden, J.S., Barton, K., Schlub, T.E., Lee, E., von Stockenstrom, S., Odevall, L., Milush, J.M., Liegler, T., et al. (2017). Identification of Genetically Intact HIV-1 Proviruses in Specific CD4$^+$ T Cells from Effectively Treated Participants. Cell Rep. *21*, 813–822.

Ho, Y.C., Shan, L., Hosmane, N.N., Wang, J., Laskey, S.B., Rosenbloom, D.I., Lai, J., Blankson, J.N., Siliciano, J.D., and Siliciano, R.F. (2013). Replication-competent noninduced proviruses in the latent reservoir increase barrier to HIV-1 cure. Cell *155*, 540–551.

Hoang, T.N., Pino, M., Boddapati, A.K., Viox, E.G., Starke, C.E., Upadhyay, A.A., Gumber, S., Nekorchuk, M., Busman-Sahay, K., Strongin, Z., et al. (2021). Baricitinib treatment resolves lower-airway macrophage inflammation and neutrophil recruitment in SARS-CoV-2-infected rhesus macaques. Cell *184*, 460–475.

Hosmane, N.N., Kwon, K.J., Bruner, K.M., Capoferri, A.A., Beg, S., Rosenbloom, D.I., Keele, B.F., Ho, Y.C., Siliciano, J.D., and Siliciano, R.F. (2017). Proliferation of latently infected CD4$^+$ T cells carrying replication-competent HIV-1: Potential role in latent reservoir dynamics. J. Exp. Med. *214*, 959–972.

Hu, Y., Hase, T., Li, H.P., Prabhakar, S., Kitano, H., Ng, S.K., Ghosh, S., and Wee, L.J. (2016). A machine learning approach for the identification of key markers involved in brain development from single-cell transcriptomic data. BMC Genomics *17* (*Suppl 13*), 1025.

Hunt, P.W., Martin, J.N., Sinclair, E., Epling, L., Teague, J., Jacobson, M.A., Tracy, R.P., Corey, L., and Deeks, S.G. (2011). Valganciclovir reduces T cell activation in HIV-infected individuals with incomplete CD4+ T cell recovery on antiretroviral therapy. J. Infect. Dis. *203*, 1474–1483.

Iezzi, G., Karjalainen, K., and Lanzavecchia, A. (1998). The duration of antigenic stimulation determines the fate of naive and effector T cells. Immunity *8*, 89–95.

Jain, V., Hartogensis, W., Bacchetti, P., Hunt, P.W., Hatano, H., Sinclair, E., Epling, L., Lee, T.H., Busch, M.P., McCune, J.M., et al. (2013). Antiretroviral therapy initiated within 6 months of HIV infection is associated with lower T-cell activation and smaller HIV reservoir size. J. Infect. Dis. *208*, 1202–1211.

Kazer, S.W., Aicher, T.P., Muema, D.M., Carroll, S.L., Ordovas-Montanes, J., Miao, V.N., Tu, A.A., Ziegler, C.G.K., Nyquist, S.K., Wong, E.B., et al. (2020). Integrated single-cell analysis of multicellular immune dynamics during hyperacute HIV-1 infection. Nat. Med. *26*, 511–518.

King Thomas, J., Mir, H., Kapur, N., and Singh, S. (2019). Racial Differences in Immunological Landscape Modifiers Contributing to Disparity in Prostate Cancer. Cancers (Basel) *11*, 1857.

Korotkevich, G., Sukhov, V., Buden, N., Shpak, B., Artyomov, M.N., and Sergushichev, A. (2019). Fast gene set enrichment analysis. Preprint at bioRxiv. https://doi.org/10.1101/060012.

Korsunsky, I., Millard, N., Fan, J., Slowikowski, K., Zhang, F., Wei, K., Baglaenko, Y., Brenner, M., Loh, P.R., and Raychaudhuri, S. (2019). Fast, sensitive and accurate integration of single-cell data with Harmony. Nat. Methods *16*, 1289–1296.

Krämer, A., Green, J., Pollard, J., Jr., and Tugendreich, S. (2014). Causal analysis approaches in Ingenuity Pathway Analysis. Bioinformatics *30*, 523–530.

Lama, J.R., Brezak, A., Dobbins, J.G., Sanchez, H., Cabello, R., Rios, J., Bain, C., Ulrich, A., De la Grecca, R., Sanchez, J., and Duerr, A. (2018). Design Strategy of the Sabes Study: Diagnosis and Treatment of Early HIV Infection Among Men Who Have Sex With Men and Transgender Women in Lima, Peru, 2013-2017. Am. J. Epidemiol. *187*, 1577–1585.

Lama, J.R., Ignacio, R.A.B., Alfaro, R., Rios, J., Cartagena, J.G., Valdez, R., Bain, C., Barbarán, K.S., Villaran, M.V., Pilcher, C.D., et al. (2021). Clinical and Immunologic Outcomes after Immediate or Deferred Antiretroviral Therapy Initiation during Primary HIV Infection: The Sabes Randomized Clinical Study. Clin Infect Dis. *72*, 1042–1050.

Langfelder, P., and Horvath, S. (2008). WGCNA: an R package for weighted correlation network analysis. BMC Bioinformatics *9*, 559.

Lee, G.Q., Orlova-Fink, N., Einkauf, K., Chowdhury, F.Z., Sun, X., Harrington, S., Kuo, H.H., Hua, S., Chen, H.R., Ouyang, Z., et al. (2017). Clonal expansion of genome-intact HIV-1 in functionally polarized Th1 CD4+ T cells. J. Clin. Invest. *127*, 2689–2696.

Lee, E., Bacchetti, P., Milush, J., Shao, W., Boritz, E., Douek, D., Fromentin, R., Liegler, T., Hoh, R., Deeks, S.G., et al. (2019). Memory CD4 + T-Cells Expressing HLA-DR Contribute to HIV Persistence During Prolonged Antiretroviral Therapy. Front. Microbiol. *10*, 2214.

Lemaître, G., Nogueira, F., and Aridas, C.K. (2017). Imbalanced-learn: A Python Toolbox to Tackle the Curse of Imbalanced Datasets in Machine Learning. J. Mach. Learn. Res. *18*, 559–563.

Liberzon, A., Subramanian, A., Pinchback, R., Thorvaldsdóttir, H., Tamayo, P., and Mesirov, J.P. (2011). Molecular signatures database (MSigDB) 3.0. Bioinformatics *27*, 1739–1740.

Liu, R., Yeh, Y.J., Varabyou, A., Collora, J.A., Sherrill-Mix, S., Talbot, C.C., Jr., Mehta, S., Albrecht, K., Hao, H., Zhang, H., et al. (2020). Single-cell transcriptional landscapes reveal HIV-1-driven aberrant host gene transcription as a potential therapeutic target. Sci. Transl. Med. *12*, eaaz0802.

Lorenzi, J.C., Cohen, Y.Z., Cohn, L.B., Kreider, E.F., Barton, J.P., Learn, G.H., Oliveira, T., Lavine, C.L., Horwitz, J.A., Settler, A., et al. (2016). Paired quantitative and qualitative assessment of the replication-competent HIV-1 reservoir and comparison with integrated proviral DNA. Proc. Natl. Acad. Sci. USA *113*, E7908–E7916.

Macallan, D.C., Busch, R., and Asquith, B. (2019). Current estimates of T cell kinetics in humans. Curr. Opin. Syst. Biol. *18*, 77–86.

Malandro, N., Budhu, S., Kuhn, N.F., Liu, C., Murphy, J.T., Cortez, C., Zhong, H., Yang, X., Rizzuto, G., Altan-Bonnet, G., et al. (2016). Clonal Abundance of Tumor-Specific CD4(+) T Cells Potentiates Efficacy and Alters Susceptibility to Exhaustion. Immunity *44*, 179–193.

Maldarelli, F., Wu, X., Su, L., Simonetti, F.R., Shao, W., Hill, S., Spindler, J., Ferris, A.L., Mellors, J.W., Kearney, M.F., et al. (2014). HIV latency. Specific HIV integration sites are linked to clonal expansion and persistence of infected cells. Science *345*, 179–183.

McGary, C.S., Deleage, C., Harper, J., Micci, L., Ribeiro, S.P., Paganini, S., Kuri-Cervantes, L., Benne, C., Ryan, E.S., Balderas, R., et al. (2017). CTLA-4$^+$PD-1$^-$ Memory CD4$^+$ T Cells Critically Contribute to Viral Persistence in Antiretroviral Therapy-Suppressed, SIV-Infected Rhesus Macaques. Immunity *47*, 776–788.e5.

McInnes, L., Healy, J., and Melville, J. (2018). UMAP: Uniform Manifold Approximation and Projection for Dimension Reduction. Preprint at arXiv. https://doi.org/10.48550/arXiv.1802.03426.

Meckiff, B.J., Ramírez-Suástegui, C., Fajardo, V., Chee, S.J., Kusnadi, A., Simon, H., Eschweiler, S., Grifoni, A., Pelosi, E., Weiskopf, D., et al. (2020). Imbalance of Regulatory and Cytotoxic SARS-CoV-2-Reactive CD4$^+$ T Cells in COVID-19. Cell *183*, 1340–1353.e16.

Mellors, J.W., Guo, S., Naqvi, A., Brandt, L.D., Su, L., Sun, Z., Joseph, K.W., Demirov, D., Halvas, E.K., Butcher, D., et al. (2021). Insertional activation of *STAT3* and *LCK* by HIV-1 proviruses in T cell lymphomas. Sci Adv. *7*, eabi8795.

Mendoza, P., Jackson, J.R., Oliveira, T.Y., Gaebler, C., Ramos, V., Caskey, M., Jankovic, M., Nussenzweig, M.C., and Cohn, L.B. (2020). Antigen-responsive CD4+ T cell clones contribute to the HIV-1 latent reservoir. J. Exp. Med. *217*, e20200051.

Morou, A., Brunet-Ratnasingham, E., Dubé, M., Charlebois, R., Mercier, E., Darko, S., Brassard, N., Nganou-Makamdop, K., Arumugam, S., Gendron-Lepage, G., et al. (2019). Altered differentiation is central to HIV-specific CD4$^+$ T cell dysfunction in progressive disease. Nat. Immunol. *20*, 1059–1070.

Ndhlovu, Z.M., Kazer, S.W., Nkosi, T., Ogunshola, F., Muema, D.M., Anmole, G., Swann, S.A., Moodley, A., Dong, K., Reddy, T., et al. (2019). Augmentation of HIV-specific T cell function by immediate treatment of hyperacute HIV-1 infection. Sci. Transl. Med. *11*, eaau0528.

Neidleman, J., Luo, X., Frouard, J., Xie, G., Hsiao, F., Ma, T., Morcilla, V., Lee, A., Telwatte, S., Thomas, R., et al. (2020). Phenotypic analysis of the unstimulated in vivo HIV CD4 T cell reservoir. eLife *9*, e60933.

Nguyen, S., Deleage, C., Darko, S., Ransier, A., Truong, D.P., Agarwal, D., Japp, A.S., Wu, V.H., Kuri-Cervantes, L., Abdel-Mohsen, M., et al. (2019). Elite control of HIV is associated with distinct functional and transcriptional signatures in lymphoid tissue $CD8^+$ T cells. Sci. Transl. Med. *11*, eaax4077.

Oh, D.Y., Kwek, S.S., Raju, S.S., Li, T., McCarthy, E., Chow, E., Aran, D., Ilano, A., Pai, C.S., Rancan, C., et al. (2020). Intratumoral CD4(+) T Cells Mediate Anti-tumor Cytotoxicity in Human Bladder Cancer. Cell. *181*, 1612–1625.e1613.

Pape, K.A., Khoruts, A., Mondino, A., and Jenkins, M.K. (1997). Inflammatory cytokines enhance the in vivo clonal expansion and differentiation of antigen-activated CD4+ T cells. J. Immunol. *159*, 591–598.

Pappalardo, J.L., Zhang, L., Pecsok, M.K., Perlman, K., Zografou, C., Raddassi, K., Abulaban, A., Krishnaswamy, S., Antel, J., van Dijk, D., and Hafler, D.A. (2020). Transcriptomic and clonal characterization of T cells in the human central nervous system. Sci. Immunol. *5*, eabb8786.

Park, M., Vorperian, S., Wang, S., and Pisco, A.O. (2020). Single-cell identity definition using random forests and recursive feature elimination. Preprint at bioRxiv. https://doi.org/10.1101/2020.08.03.233650.

Pedregosa, F., Varoquaux, G., Gramfort, A., Michel, V., Thirion, B., Grisel, O., Blondel, M., Prettenhofer, P., Weiss, R., Dubourg, V., Vanderplas, J., et al. (2011). Scikit-learn: Machine Learning in Python. J. Mach. Learn. Res. *12*, 2825–2830.

Pollack, R.A., Jones, R.B., Pertea, M., Bruner, K.M., Martin, A.R., Thomas, A.S., Capoferri, A.A., Beg, S.A., Huang, S.H., Karandish, S., et al. (2017). Defective HIV-1 Proviruses Are Expressed and Can Be Recognized by Cytotoxic T Lymphocytes, which Shape the Proviral Landscape. Cell Host Microbe *21*, 494–506.e4.

R Core Team (2021). R: A language and environment for statistical computing (Vienna, Austria: R Foundation for Statistical Computing). https://www.R-project.org/.

Ren, Y., Huang, S.H., Patel, S., Alberto, W.D.C., Magat, D., Ahimovic, D., Macedo, A.B., Durga, R., Chan, D., Zale, E., et al. (2020). BCL-2 antagonism sensitizes cytotoxic T cell-resistant HIV reservoirs to elimination ex vivo. J. Clin. Invest. *130*, 2542–2559.

Shalek, A.K., Satija, R., Adiconis, X., Gertner, R.S., Gaublomme, J.T., Raychowdhury, R., Schwartz, S., Yosef, N., Malboeuf, C., Lu, D., et al. (2013). Single-cell transcriptomics reveals bimodality in expression and splicing in immune cells. Nature *498*, 236–240.

Siliciano, J.D., Kajdas, J., Finzi, D., Quinn, T.C., Chadwick, K., Margolick, J.B., Kovacs, C., Gange, S.J., and Siliciano, R.F. (2003). Long-term follow-up studies confirm the stability of the latent reservoir for HIV-1 in resting CD4+ T cells. Nat. Med. *9*, 727–728.

Simonetti, F.R., Sobolewski, M.D., Fyne, E., Shao, W., Spindler, J., Hattori, J., Anderson, E.M., Watters, S.A., Hill, S., Wu, X., et al. (2016). Clonally expanded CD4+ T cells can produce infectious HIV-1 in vivo. Proc. Natl. Acad. Sci. USA *113*, 1883–1888.

Simonetti, F.R., Zhang, H., Soroosh, G.P., Duan, J., Rhodehouse, K., Hill, A.L., Beg, S.A., McCormick, K., Raymond, H.E., Nobles, C.L., et al. (2021). Antigen-driven clonal selection shapes the persistence of HIV-1-infected CD4+ T cells in vivo. J. Clin. Invest. *131*, e145254.

Stout-Delgado, H.W., Getachew, Y., Rogers, T.E., Miller, B.C., and Thiele, D.L. (2007). The role of serpinb9/serine protease inhibitor 6 in preventing granzyme B-dependent hepatotoxicity. Hepatology *46*, 1530–1540.

Stuart, T., Butler, A., Hoffman, P., Hafemeister, C., Papalexi, E., Mauck, W.M., 3rd, Hao, Y., Stoeckius, M., Smibert, P., and Satija, R. (2019). Comprehensive Integration of Single-Cell Data. Cell. *177*, 1888–1902.e1821.

Tirosh, I., Izar, B., Prakadan, S.M., Wadsworth, M.H., 2nd, Treacy, D., Trombetta, J.J., Rotem, A., Rodman, C., Lian, C., Murphy, G., et al. (2016). Dissecting the multicellular ecosystem of metastatic melanoma by single-cell RNA-seq. Science *352*, 189–196.

Torang, A., Gupta, P., and Klinke, D.J., 2nd (2019). An elastic-net logistic regression approach to generate classifiers and gene signatures for types of immune cells and T helper cell subsets. BMC Bioinformatics *20*, 433.

van Leeuwen, E.M., Remmerswaal, E.B., Vossen, M.T., Rowshani, A.T., Wertheim-van Dillen, P.M., van Lier, R.A., and ten Berge, I.J. (2004). Emergence of a CD4+CD28- granzyme B+, cytomegalovirus-specific T cell subset after recovery of primary cytomegalovirus infection. J. Immunol. *173*, 1834–1841.

Vander Heiden, J.A., Yaari, G., Uduman, M., Stern, J.N., O'Connor, K.C., Hafler, D.A., Vigneault, F., and Kleinstein, S.H. (2014). pRESTO: a toolkit for processing high-throughput sequencing raw reads of lymphocyte receptor repertoires. Bioinformatics *30*, 1930–1932.

Venanzi Rullo, E., Pinzone, M.R., Cannon, L., Weissman, S., Ceccarelli, M., Zurakowski, R., Nunnari, G., and O'Doherty, U. (2020). Persistence of an intact HIV reservoir in phenotypically naive T cells. JCI Insight *5*, e133157.

Vogler, M. (2012). BCL2A1: the underdog in the BCL2 family. Cell Death Differ. *19*, 67–74.

Wagner, T.A., McLaughlin, S., Garg, K., Cheung, C.Y., Larsen, B.B., Styrchak, S., Huang, H.C., Edlefsen, P.T., Mullins, J.I., and Frenkel, L.M. (2014). HIV latency. Proliferation of cells with HIV integrated into cancer genes contributes to persistent infection. Science *345*, 570–573.

Wang, Z., Gurule, E.E., Brennan, T.P., Gerold, J.M., Kwon, K.J., Hosmane, N.N., Kumar, M.R., Beg, S.A., Capoferri, A.A., Ray, S.C., et al. (2018). Expanded cellular clones carrying replication-competent HIV-1 persist, wax, and wane. Proc. Natl. Acad. Sci. USA *115*, E2575–E2584.

Wilk, A.J., Rustagi, A., Zhao, N.Q., Roque, J., Martínez-Colón, G.J., McKechnie, J.L., Ivison, G.T., Ranganath, T., Vergara, R., Hollis, T., et al. (2020). A single-cell atlas of the peripheral immune response in patients with severe COVID-19. Nat. Med. *26*, 1070–1076.

Wong, J.K., Hezareh, M., Günthard, H.F., Havlir, D.V., Ignacio, C.C., Spina, C.A., and Richman, D.D. (1997). Recovery of replication-competent HIV despite prolonged suppression of plasma viremia. Science *278*, 1291–1295.

Yeh, Y.J., Jenike, K.M., Calvi, R.M., Chiarella, J., Hoh, R., Deeks, S.G., and Ho, Y.C. (2020). Filgotinib suppresses HIV-1-driven gene transcription by inhibiting HIV-1 splicing and T cell activation. J. Clin. Invest. *130*, 4969–4984.

Yost, K.E., Satpathy, A.T., Wells, D.K., Qi, Y., Wang, C., Kageyama, R., McNamara, K.L., Granja, J.M., Sarin, K.Y., Brown, R.A., et al. (2019). Clonal replacement of tumor-specific T cells following PD-1 blockade. Nat. Med. *25*, 1251–1259.

Zaunders, J.J., Dyer, W.B., Wang, B., Munier, M.L., Miranda-Saksena, M., Newton, R., Moore, J., Mackay, C.R., Cooper, D.A., Saksena, N.K., and Kelleher, A.D. (2004). Identification of circulating antigen-specific CD4+ T lymphocytes with a CCR5+, cytotoxic phenotype in an HIV-1 long-term nonprogressor and in CMV infection. Blood *103*, 2238–2247.

Zhang, M., Park, S.-M., Wang, Y., Shah, R., Liu, N., Murmann, A.E., Wang, C.-R., Peter, M.E., and Ashton-Rickardt, P.G. (2006). Serine protease inhibitor 6 protects cytotoxic T cells from self-inflicted injury by ensuring the integrity of cytotoxic granules. Immunity *24*, 451–461.

Zhou, H., and Hastie, T. (2005). Regularization and variable selection via the Elastic Net. J. R. Stat. Soc. B *67*, 301–320.

Please cite this article in press as: Collora et al., Single-cell multiomics reveals persistence of HIV-1 in expanded cytotoxic T cell clones, Immunity (2022), https://doi.org/10.1016/j.immuni.2022.03.004

STAR★METHODS

KEY RESOURCES TABLE

REAGENT or RESOURCE	SOURCE	IDENTIFIER
Antibodies		
CD8-BV510 clone SK1	BioLegend	CAT# 344731; RRID:AB_2564623
CD14-BV510 clone M5E2	BioLegend	CAT# 301841; RRID:AB_2561379
CD19-BV510 clone HIB19	BioLegend	CAT# 302241; RRID:AB_2561381
CD56-BV510 clone 5.1H11	BioLegend	CAT# 362533; RRID:AB_2565632
CD3-BV421 clone SK7	BioLegend	CAT# 344833; RRID:AB_2565674
CD69-BV650 clone FN50	BioLegend	CAT# 310933; RRID:AB_2561783
CD154-PE clone 24-31	BioLegend	CAT# 310805; RRID:AB_314828
CD45RO-APC/Fire750 clone UCHL1	BioLegend	CAT# 304249; RRID:AB_2616716
TotalSeq-C IL7RA clone A019D5	BioLegend	CAT# 351356; RRID:AB_2800937
TotalSeq-C CCR7 clone G043H7	BioLegend	CAT# 353251; RRID:AB_2800943
TotalSeq-C CD25 clone BC96	BioLegend	CAT# 302649; RRID:AB_2800745
TotalSeq-C CD27 clone O323	BioLegend	CAT# 302853; RRID:AB_2800747
TotalSeq-C CD3 clone UCHT1	BioLegend	CAT# 300479; RRID:AB_2800723
TotalSeq-C CD4 clone RPA-T4	BioLegend	CAT# 300567; RRID:AB_2800725
TotalSeq-C CD8 clone RPA-T8	BioLegend	CAT# 301071; RRID:AB_2800730
TotalSeq-C CD45RA clone HI100	BioLegend	CAT# 304163; RRID:AB_2800764
TotalSeq-C CD45RO clone UCHL1	BioLegend	CAT# 304259; RRID:AB_2800766
TotalSeq-C CD62L clone DREG-56	BioLegend	CAT# 304851; RRID:AB_2800770
TotalSeq-C CD69 clone FN50	BioLegend	CAT# 310951; RRID:AB_2800810
TotalSeq-C HLA-DR clone L243	BioLegend	CAT# 307663; RRID:AB_2800795
TotalSeq-C CD47 clone CC2C6	BioLegend	CAT# 323131; RRID:AB_2810482
TotalSeq-C CCR5 clone J418F1	BioLegend	CAT# 359137; RRID:AB_2810570
TotalSeq-C CXCR3 clone G025H7	BioLegend	CAT# 353747; RRID:AB_2800949
TotalSeq-C CCR6 clone G034E3	BioLegend	CAT# 353440; RRID:AB_2810563
TotalSeq-C CCR4 clone L291H4	BioLegend	CAT# 359425; RRID:AB_2800988
TotalSeq-C CXCR5 clone J252D4	BioLegend	CAT# 356939; RRID:AB_2800968
TotalSeq-C CD40L clone 24-31	BioLegend	CAT# 310849; RRID:AB_2800808
TotalSeq-C 4-1BB clone 4B4-1	BioLegend	CAT# 309839; RRID:AB_2800807
TotalSeq-C OX40 clone ACT35	BioLegend	CAT# 350035; RRID:AB_2800932
TotalSeq-C PD-1 clone EH12.2H7	BioLegend	CAT# 329963; RRID:AB_2800862
TotalSeq-C CTLA-4 clone BNI3	BioLegend	CAT# 369621; RRID:AB_2801015
TotalSeq-C TIGIT clone A15153G	BioLegend	CAT# 372729; RRID:AB_2801021
TotalSeq-C mouse IgG1 clone MOPC-21	BioLegend	CAT# 400187; RRID:AB_2888921
TotalSeq-C mouse IgG2a clone MOPC-173	BioLegend	CAT# 400293; RRID:AB_2888922
TotalSeq-C mouse IgG2b clone MPC-11	BioLegend	CAT# 400381; RRID:AB_2888923
TotalSeq-C human hashing antibody 1	BioLegend	CAT# 394661; RRID:AB_2801031
TotalSeq-C human hashing antibody 2	BioLegend	CAT# 394663; RRID:AB_2801032
TotalSeq-C human hashing antibody 3	BioLegend	CAT# 394665; RRID:AB_2801033
TotalSeq-C human hashing antibody 4	BioLegend	CAT# 394667; RRID:AB_2801034
TotalSeq-C human hashing antibody 5	BioLegend	CAT# 394669; RRID:AB_2801035
TotalSeq-C human hashing antibody 6	BioLegend	CAT# 394671; RRID:AB_2820042
TotalSeq-C human hashing antibody 7	BioLegend	CAT# 394673; RRID:AB_2820043
TotalSeq-C human hashing antibody 8	BioLegend	CAT# 394675; RRID:AB_2820044
TotalSeq-C human hashing antibody 9	BioLegend	CAT# 394677; RRID:AB_2820045

(*Continued on next page*)

Please cite this article in press as: Collora et al., Single-cell multiomics reveals persistence of HIV-1 in expanded cytotoxic T cell clones, Immunity (2022), https://doi.org/10.1016/j.immuni.2022.03.004

Continued

REAGENT or RESOURCE	SOURCE	IDENTIFIER
TotalSeq-C human hashing antibody 10	BioLegend	CAT# 394679; RRID:AB_2820046
CD45RA-BUV737 clone HI100	BD Biosciences	CAT# 612846; RRID:AB_2870168
CCR7-BUV395 clone 3D12	BD Biosciences	CAT# 740267; RRID:AB_2740009
CTLA4-PE-Dazzel594 clone L3D10	Bioledgend	CAT# 349921; RRID:AB_2566197
IFNG-BV711 clone 4S.B3	BD Biosciences	CAT# 564793; RRID:AB_2738953
TNF-BV605 clone Mab11	Biolegend	CAT# 502935; RRID:AB_11203719
p24-PE clone KC57	Beckman Coulter	CAT# 6604667; RRID:AB_1575989
p24-APC clone 28B7	Medimabs	CAT# MM-0289-APC
GZMB-AF700 GB11	BD Biosciences	CAT# 561016; RRID:AB_2033973
Biological samples		
Demographics of study participants, see Table S1	This paper	N/A
Human serum	Sigma Aldrich	CAT# H4522-20ML
Chemicals, peptides, and recombinant proteins		
Staphylococcal enterotoxin type B (SEB) toxin	List Biological Laboratories	CAT# 122
HIV-1 group B Gag, Pol, Env, and Nef peptide pools	NIH HIV Reagent Program	CAT# 12425, 12438, 12540, 12545
CMV lysate, strain AD-169	ZeptoMetrix	CAT# 810003
HCMV pp65 peptide pool	NIH HIV Reagent Program	CAT# 11549
enfuvirtide	NIH HIV Reagent Program	CAT# 12732
Ionomycin	Millipore	CAT# 407950-1MG
PMA	Millipore	CAT# 5.00582.0001
Brefeldin A	Thermo Fisher Scientific	CAT# 00-4506-51
Monensin	Thermo Fisher Scientific	CAT# 00-4505-51
CD40 antibody	Miltenyi Biotech	CAT# 130-094-133
Critical commercial assays		
Chromium Next GEM Single Cell 5¢ Library & Gel Bead Kit v1.1	10x Genomics	PN-1000165
Chromium Single Cell V(D)J Enrichment Kit, Human T Cell	10x Genomics	PN-1000005
Chromium Single Cell 5¢ Feature Barcode Library Kit	10x Genomics	PN-1000080
NEBNext Immune Sequencing Kit	New England Biolabs	CAT# E6320S
EasySep Direct Human $CD4^+$ T cell kit	STEM CELL	19662
CD4 T cell isolation kit, human	Miltenyi Biotech	130-096-533
EasySep Dead Cell Removal (Annexin V) Kit	STEMCELL	17899
Dynabead CD8	Thermo Fisher	11147D
LIVE/DEAD Fixable Aqua Dead Cell Stain Kit	Thermo Fisher	L34957
LIVE/DEAD Fixable Near-IR Dead Cell Stain Kit	Thermo Fisher	L10119
Deposited data		
ECCITE-seq unstimulated $CD4^+$ T cells	This study	GEO: GSE187515
ECCITE-seq stimulated $CD4^+$ T cells	This study	GEO: GSE187515
Bulk TCR repertoire profiling from HIV-1 infected and uninfected individuals	This study	GEO: GSE187515
Software and algorithms		
cellranger count version 3.0.2	10X Genomics	https://support.10xgenomics.com/single-cell-gene-expression/software/downloads/3.0/

(*Continued on next page*)

Please cite this article in press as: Collora et al., Single-cell multiomics reveals persistence of HIV-1 in expanded cytotoxic T cell clones, Immunity (2022), https://doi.org/10.1016/j.immuni.2022.03.004

Continued

REAGENT or RESOURCE	SOURCE	IDENTIFIER
cellranger vdj version 3.1	10X Genomics	https://support.10xgenomics.com/single-cell-gene-expression/software/downloads/3.1/
Seurat version 4.0.3	Stuart et al., 2019	https://cran.r-project.org/web/packages/Seurat/index.html
batchelor version 1.6.3	Haghverdi et al., 2018	https://www.bioconductor.org/packages/release/bioc/html/batchelor.html
uwot version 0.1.10	N/A	https://cran.r-project.org/web/packages/uwot/index.html
STAR version 2.5.3	Dobin et al., 2013	https://github.com/alexdobin/STAR
WGCNA version 1.70-3	Langfelder and Horvath, 2008	https://cran.r-project.org/web/packages/WGCNA/index.html
pRESTO version 0.6.1	Vander Heiden et al., 2014	https://presto.readthedocs.io/en/stable/
ChangeO version 1.0.0	Gupta et al., 2015	https://changeo.readthedocs.io/en/stable/
scikit-learn version 0.23	Pedregosa et al., 2011	https://scikit-learn.org/stable/
IPA summer 2021 release	Krämer et al., 2014	https://digitalinsights.qiagen.com/products-overview/discovery-insights-portfolio/analysis-and-visualization/qiagen-ipa/
scRFE, version 1.5.6	Park et al., 2020	https://github.com/czbiohub/scRFE
Imbalanced-learn version 0.7.0	Lemaître et al., 2017	https://imbalanced-learn.org/stable/
fGSEA version 1.16.0	Korotkevich et al., 2019	http://bioconductor.org/packages/release/bioc/html/fgsea.html
R version 4.0.3	R Core Team (2021)	https://www.r-project.org/
CodonCode version 7	CodonCode Corporation	https://www.codoncode.com/aligner/
Analysis scripts	This paper	https://github.com/Ya-ChiHo/Collora-and-Liu-et-al-2022

RESOURCE AVAILABILITY

Lead contact

Further information and requests for resources and reagents should be directed to and will be fulfilled by the lead contact Ya-Chi Ho (ya-chi.ho@yale.edu).

Materials availability

This study did not generate new unique reagents.

Data and code availability

Single-cell RNA-seq, and bulk TCR sequencing data have been deposited at GEO (GEO: GSE187515) and are publicly available. Accession numbers are listed in the key resources table. All original code has been deposited at Github and is publicly available. DOIs are listed in the key resources table. Any additional information required to reanalyze the data reported in this paper is available from the lead contact upon request.

EXPERIMENTAL MODEL AND SUBJECT DETAILS

Study participants

The demographics of the study participants are listed in Table S1. The Sabes and MERLIN studies were reviewed and approved by the Institutional Review Board (IRB) at the Fred Hutchinson Cancer Research Center and the non-government organization Asociación Civil Impacta Salud y Educación, Lima, Perú (Impacta) as well as by the ethics committee of Impacta and the Peruvian National Institute of Health. Specimen collection from Yale University and Wistar Institute was reviewed and approved by the IRB at Yale University and Wistar Institute, respectively. All participants provided written informed consent, including consent for storage and future use of specimens.

For paired blood samples during viremia and after viral suppression, participants were recruited under the Sabes study protocol and viably frozen peripheral blood mononuclear cells (PBMC) were obtained under the MERLIN study protocol (Lama et al., 2018, 2021). Briefly, uninfected study participants were prospectively tested monthly by third-generation HIV-1 antibody

Please cite this article in press as: Collora et al., Single-cell multiomics reveals persistence of HIV-1 in expanded cytotoxic T cell clones, Immunity (2022), https://doi.org/10.1016/j.immuni.2022.03.004

immunoassays. Seronegative samples were tested for HIV-1 RNA with pooled nucleic acid amplification (NAAT) tests. Participants with incident HIV-1 infection were rapidly linked to the next phase of the study. After specimen collection during viremia (viremic samples with a documented viral load), participants were randomly assigned to immediate and deferred ART initiation arms. In the immediate ART arm, participants initiated ART (either EFV/FTC/TDF or EGV/COBI/FTC/TDF) at the baseline visit (< 2 months of estimated date of infection (Lama et al., 2021)). In the deferred ART arm, participants initiated ART 24 weeks after the baseline visit (6–8 months after estimated date of infection). After one year of suppressive ART (documented by a plasma viral load < 200 copies/mL at 6 months prior to blood sampling), the virally suppressed specimens were taken. We obtained blood samples from 3 individuals from the immediate ART arm and three individuals from the deferred ART arm to ensure our results are generalizable to different treatment conditions.

For uninfected controls, two sex-matched HIV-1-uninfected individuals were recruited at Yale University. For flow cytometry validation studies, eight sex-matched HIV-1-infected individuals under long-term suppressive ART (mean 75 months, range 41–182 months) were recruited at Wistar institute.

METHOD DETAILS

Isolation of unstimulated and antigen-specific CD4$^+$ T cells

For unstimulated CD4$^+$ T cells, aliquots of 20 million PBMCs were thawed. Dead cells were removed by magnetic depletion (STEMCELL Technologies). CD4$^+$ T cells were purified with magnetic negative selection (Miltenyi Biotec) and stained with Total-Seq C antibodies (BioLegend). Antigen-specific CD4$^+$ T cells were isolated from cryopreserved PBMC following activation induced marker (AIM) protocols as previously described (Morou et al., 2019). CD8$^+$ T cells were depleted (using CD8 Dynabeads, Thermo Fisher) to prevent CD8 killing of HIV-1-infected CD4$^+$ T cells during activation. CD8-depleted PBMCs were aliquoted as 15 million cells per well in 24-well plates in RPMI media supplemented with 10% human serum (Sigma-Aldrich). Cells were rested at 37 °C incubator for 3 h. 15 min before stimulation, 0.5 μg/mL CD40 antibody (Miltenyi Biotec) was added to reduce CD40L internalization. Cells were stimulated with an overlapping peptide pool corresponding to HIV-1 group B Gag, Pol, Env, and Nef (1 μg/mL per peptide, NIH HIV Reagent Program) for HIV-1 antigen stimulation. For CMV antigen stimulation, cells were stimulated with CMV lysate (1 μg/mL, ZeptoMetrix) and an overlapping peptide pool corresponding to HCMV pp65 (1 μg/mL per peptide, NIH HIV Reagent Program). 10 μM enfuvirtide (T20) was added to each well to prevent new infection events *in vitro*. For each assay, aliquots of PBMC were stimulated with DMSO as a negative control and with Staphylococcal enterotoxin type B (SEB) toxin (1 μg/mL, List Biological Laboratories) as a positive control. After 9 h stimulation, cells were stained for viability using LIVE/DEAD Fixable Aqua Dead Cell Stain Kit (Thermo Fisher) and a panel of antibodies against CD8 (BV510, BioLegend, clone SK1), CD14 (BV510, BioLegend, clone M5E2), CD19 (BV510, BioLegend, clone HIB19), CD56 (BV510, BioLegend, clone NCAM), CD3 (BV421, BioLegend, clone SK7), CD69 (BV650, BioLegend, clone FN50), CD154 (PE, BioLegend, clone 24-31), and CD45RO (APC/Fire750, BioLegend, clone UCHL1) in Brilliant Stain Buffer (BD Biosciences). CD69 and CD154 double positive CD4$^+$ T cells were sorted by flow cytometry as antigen-specific cells. CD69 and CD154 double negative, CD45RO positive cells were sorted as memory CD4$^+$ T cells that did not respond to HIV-1 or CMV antigen stimulations. All cells were sorted on a BD FACSAria Flow Cytometer (BD Biosciences) into tubes containing RPMI media with 20% fetal bovine serum, 25 mM HEPES, 50 U/mL penicillin, and 50 μg/mL streptomycin (Thermo Fisher). Sorted cells were pelleted and stained with Total-Seq C antibodies (BioLegend).

DNA-barcoded surface protein staining

CD4$^+$ T cells from four participants (236, 829, 739, and 799) in unstimulated conditions and all participants in the antigen stimulated conditions were stained with a full panel of 24 surface protein markers [IL7RA (clone A019D5), CCR7 (clone G043H7), CD25 (clone BC96), CD27 (clone O323), CD3 (clone UCHT1), CD4 (clone RPA-T4), CD8 (clone RPA-T8), CD45RA (clone HI100), CD45RO (clone UCHL1), CD62L (clone DREG-56), CD69 (clone FN50), HLA-DR clone (L243), CD47 (clone CC2C6), CCR5 (clone J418F1), CXCR3 (clone G025H7), CCR6 (clone G034E3), CCR4 (clone L291H4), CXCR5 (clone J252D4), CD40L (clone 24-31), 4-1BB (clone 4B4-1), OX40 (clone ACT35), PD-1 (clone EH12.2H7), CTLA-4 (clone BNI3), and TIGIT (clone A15153G)] and three isotype control staining antibodies [mouse IgG1 (clone MOPC-21), mouse IgG2a (clone MOPC-173), and mouse IgG2b (clone MPC-11)]. CD4$^+$ T cells from antigen stimulated conditions were additionally stained with anti-human Hashtag antibodies (BioLegend Total-seq C) for sample pooling. CD4$^+$ T cells from four individuals (M2, M3, 640, and 910) in the unstimulated condition were stained with a panel of 13 antibodies [IL7RA (clone A019D5), CCR7 (clone G043H7), CD25 (clone BC96), CD27 (clone O323), CD3 (clone UCHT1), CD4 (clone RPA-T4), CD45RA (clone HI100), CD45RO (clone UCHL1), CD62L (clone DREG-56), CD69 (clone FN50), HLA-DR (clone L243), PD-1 (clone EH12.2H7), and TIGIT (clone A15153G)] and the same three isotype control staining antibodies [mouse IgG1 (clone MOPC-21), mouse IgG2a (clone MOPC-173), and mouse IgG2b (clone MPC-11)].

ECCITE-seq library preparation and sequencing

Cells were loaded into the 10x Genomics Chromium Controller with a target capture of 10,000 single cells per sample. Library preparation for the single cell immune profiling with feature barcoding were performed according to manufacturer instructions (10x document CG000186 Rev D). Briefly, polyadenylated mRNA was reverse transcribed using poly(dT) primers and captured by template switch oligos. DNA barcodes on the surface protein staining and hashing antibodies were captured by annealing the reverse complement template switch oligo to the template switch oligo. After cDNA amplification, high molecular weight DNA was isolated for

Please cite this article in press as: Collora et al., Single-cell multiomics reveals persistence of HIV-1 in expanded cytotoxic T cell clones, Immunity (2022), https://doi.org/10.1016/j.immuni.2022.03.004

separate T cell receptor (TCR) and transcriptome library preparation, while low molecular weight DNA was used for surface antibody barcode library preparation. Libraries were then sequenced on either HiSeq 4000 or NovaSeq 6000 in appropriate read configurations.

Bulk T cell receptor library preparation and sequencing

Total RNA from aliquots of ~2 million $CD4^+$ T cells were used to capture a broader $CD4^+$ TCR repertoire using NEBNext Immune Sequencing Kit (New England Biolabs) according to manufacturer instructions. Briefly, RNA underwent reverse transcription using a UMI-labeled oligonucleotide. cDNA was universally amplified and then enriched for TCRβ chain by targeted amplification. Resulting libraries were sequenced on a MiSeq in 2x300 bp read mode.

Autologous HIV-1 sequencing

RNA transcripts from ECCITE-seq were mapped to HIV-1 genome. To increase mapping efficiency, autologous HIV-1 RNA sequences were used for mapping in addition to the HXB2 reference sequence. Autologous HIV-1 sequences from study participants were identified from the supernatant of p24 positive viral outgrowth culture wells and from near-full length limiting-dilution PCR from DNA of $CD4^+$ T cells (Ho et al., 2013). Sequences from both methods were assembled into contigs and aligned to HXB2 using CodonCode (version 7). Gaps were filled with HXB2 sequence.

Flow cytometric validation

Aliquots of 100 million (Sabes samples) or 200 million (Wistar samples) cryopreserved PBMC were thawed. $CD4^+$ T cells were isolated by negative selection (Miltenyi Biotec). Cells were cultured for 24 h in 1 μg/mL phorbol myristate acetate (PMA), 1 μM ionomycin, 30 U/mL IL-2, 3 μg/mL brefeldin A, and 2 μM monensin. 10 μM enfuvirtide (T20) was added to each well to prevent new infection events *in vitro*. Cells were then stained with a viability dye (LIVE/DEAD Fixable Near-IR Dead cell stain kit, Thermo Fisher) and surface protein antibodies [CD45RA (BUV737, BD Biosciences, clone HI100), CCR7 (BUV395, BD Biosciences, clone 3D12), CTLA4 (PE-Dazzel594, BioLegend, clone L3D10] for 30 min at 4°C in 1 mL with Brilliant Stain Buffer Plus (BD Biosciences). Cells were washed twice with wash media and fixed in 1 mL of Foxp3 Transcription Factor Staining Buffer Set (Thermo Fisher) for 45 min at room temperature according to manufacturer instructions. Cells were washed twice with permeabilization buffer and then stained with intracellular protein antibodies [IFNγ (BV711, BD Biosciences, clone 4S.B3), TNF (BV605, BioLegend, clone Mab11), p24 (PE, Beckman Coulter, clone KC57), p24 (APC, Medimabs, clone 28B7), granzyme B (AF700, BD Biosciences, GB11)] for 45 min at room temperature. Cells were washed twice with permeabilization buffer and resuspended in wash media for analysis using BD FACSAria. Flow cytometry results were analyzed using FlowJo (BD Biosciences, version 10.8.0).

Single-cell multi-omic analysis

Sequence alignment

Reads from gene expression and surface protein antibody barcode were aligned using cellranger count (10x Genomics, version 3.0.2). Reads from TCR sequencing were assembled and aligned using cellranger vdj (10x Genomics, version 3.1). Unfiltered count matrices and TCR assignments were output for downstream analysis.

Doublet discrimination

TCR sequences were used first to identify doublets as defined by > 3 productive TCR chain contigs assigned to a single cell barcode. Cells identified as doublets were removed from count matrices.

Quality control

T cell variable gene fragments were removed from consideration for variable genes. Count matrices were then used to initialize Seurat Objects (Stuart et al., 2019), with TCR data added as metadata. Cells were filtered to remove cells with greater than 10% mitochondrial gene expression or fewer than 500 genes.

Hashing antibody demultiplexing

To separate individual samples from pooled antigen specific single cell libraries, we utilized the Seurat function HTODemux on each individual library. Hashing antibody-defined doublets and barcodes without hashing assignment were discarded.

Batch effect correction by integration

Following this rough filtering, for unstimulated data two rounds of integration were performed. In the first integration step, each sample was normalized using SCTransform and integrated using fastMNN (Haghverdi et al., 2018). We chose fastMNN (as opposed to reciprocal principal component analysis in Seurat3 (Stuart et al., 2019) or Harmony (Korsunsky et al., 2019)) because this integration method preserves the biological differences between sorted $CD69^+CD154^+$ cells versus $CD69^-CD154^-$ cells without over integration. Twenty nearest neighbors in the mutual nearest neighbor space were identified and used to generate clusters with a resolution parameter of 0.4. Uniform Manifold Approximation and Projection (UMAP) was used to visualize cells in a low dimensional space (version 3) (McInnes et al., 2018). Clusters without > 50% CD3 barcoded surface antibody staining were discarded as non-T cells. Clusters with expression of *CD8A, KLRC1*, or *KLRC3* in more than 20% of cells were discarded as $CD8^+$ T cells or NKT cells. In the second integration step, the remaining cells were reintegrated using the same workflow without contaminating cells. Since the stimulated data was generated from sorted $CD4^+$ T cell populations, only a single round of integration was required with the same parameters as above.

Please cite this article in press as: Collora et al., Single-cell multiomics reveals persistence of HIV-1 in expanded cytotoxic T cell clones, Immunity (2022), https://doi.org/10.1016/j.immuni.2022.03.004

Surface protein expression analysis

Similar to flow cytometry-based antibody staining and measurement of surface protein expression, cells having higher normalized read counts of barcoded surface antibody staining, as measured by > 90th percentile of the expression level of isotype barcoded antibody controls, were defined as positive for the respective surface protein expression.

Cell type identification

Following cluster identification in the mutual nearest neighbor space with a resolution parameter of 0.4, the single-cell transcriptional landscape was plotted by UMAP (McInnes et al., 2018). Genes having > 0.25 $\log_2$ fold change difference were used in conjunction with protein expression to annotate the CD4$^+$ T cell immune phenotype of individual clusters. By examining the expression level of two surface protein expression in the same single cell, memory cell phenotype can be defined as naive (CD45RA$^+$, CCR7$^+$), central memory (CD45RA$^-$, CCR7$^+$), effector memory (CD45RA$^-$, CCR7$^-$), and effector (CD45RA$^+$, CCR7$^-$) CD4$^+$ T cells.

HIV-1 RNA$^+$ cell identification

Transcriptome reads were aligned to a compendium of autologous viruses using STAR (version 2.5.3) (Dobin et al., 2013). STAR was run in two passes, first to identify and annotate splice sites in the input HIV-1 genomes, and second to realign to the annotated genomes. No multiple mapping reads were discarded at this stage. Barcodes and UMIs were extracted from the associated reads and filtered in an R script to identify HIV-1 RNA$^+$ cells. To guard against artifacts generated by potential index hopping, cells with a minimum of 2 HIV-1-related UMI or 4 reads of a single UMI were considered positive.

Gene expression module analysis and scoring

Gene expression modules were identified as previously described (Kazer et al., 2020). Briefly, objects were subset by cell types of interest, the first 3–10 principal components were used to identify the 50 most significant genes positively and negatively associated with those components (Kazer et al., 2020). The expression matrix of those identified genes was used as input for weighted gene correlation network analysis (WGCNA, version 1.70-3)(Langfelder and Horvath, 2008). A soft power was selected per author's recommendations where possible and reduced if fewer than 3 modules of a minimum size 10 were identified. Module significance was determined by bootstrapped sampling as previously described (Kazer et al., 2020). Modules were clustered using the R function hclust to merge similar modules with a cutoff of 2.2. Modules were scored as previously described (Tirosh et al., 2016) using the Seurat function AddModuleScore. Differences between groups were identified using Wilcoxon rank-sum test.

T cell clone analysis

Reads from bulk TCR sequencing were trimmed, merged, and assembled into consensus contigs based on UMI using pRESTO (version 0.6.1) (Vander Heiden et al., 2014). Resulting contigs were aligned to a database of IGMT TCR segment genes and annotated by ChangeO (version 1.0.0) (Gupta et al., 2015). TCRs were then filtered for productive contigs. Clones were defined based on the complementarity-determining region 3 (CDR3) nucleotide junction on TCRβ by individual. Bulk frequencies were quantified, normalized to the total captured TCRs, and used to annotate the size of single TCR clones. TCRs captured by 10x Genomics TCR sequencing in single cells but not in bulk sequencing were set to singleton frequency for each individual. Cells with > 1 captured TCR from the same individuals at any time point were defined as clonal (from 595,014 unique TCRs 115,478 clones were identified in bulk. 15,004, 1,152, 1,394, and 9,285 of those clones had single cell RNA-seq derived transcriptomes in unstimulated, CMV-specific, HIV-1-specific, and sorted memory conditions respectively). Each clone was tested for significant changes between virema and viral suppression time points using Fisher's exact test. Clones with at least one cell that was HIV-1 RNA$^+$ were considered as HIV-1 RNA$^+$ T cell clone.

Permutation testing of observed HIV-1 RNA$^+$ clone size relative to overall clone size distribution

To determine if the observed increased HIV-1 RNA$^+$ clone size was due to the increased chance of observing an HIV-1 RNA$^+$ cell in a large clone as opposed to an increased size intrinsic to HIV-1 RNA$^+$ clones we implemented a permutation test. First, we determined the number of HIV-1 RNA$^+$ cells in clones detected in a given group "HIV N." We then subset all our observed cells to exclusively cells in clones (the same TCR sequence detected twice) "clonal pool." We then randomly sampled "HIV N" cells from the "clonal pool" without replacement. Cells in both the HIV group and the sampled cells were collapsed into independent clones so that no clone frequency was counted multiple times. Finally, this subset of sampled clone frequency was compared to the observed HIV-1 RNA$^+$ clone sizes using a one-tailed Wilcoxon rank-sum to determine if HIV-1 RNA$^+$ clone sizes were larger than the sampled clone sizes. This procedure was completed 10,000 times for each comparison. We considered a given relationship significant if greater than 95% of permutation comparisons were significant.

Elastic net clonal regression

To identify gene expression profile that correlate with T cell clone size, we used elastic net, a regression method that utilizes Lasso feature elimination and the coefficient reduction of Ridge regression (Zhou and Hastie, 2005). Data were split by condition. A matrix of the gene expression and clone sizes were output for from Seurat for elastic net regression in scikit-learn (Pedregosa et al., 2011) (version 0.23). Data were split 80-20 with genes serving as candidate predictive features and clone size as target data. A parameter search was used to identify an alpha value maximizing accuracy with the initial 80 split, yielding values ranging from 0.1 to 0.001. Optimal alphas were then averaged (resulting in 0.0285) and used to train final models. This resulted in accuracy scores between 0.54 and 0.83 (median 0.68) in the test set. Coefficients and gene names were output for further analysis using ingenuity pathway analysis (IPA)(Krämer et al., 2014).

Please cite this article in press as: Collora et al., Single-cell multiomics reveals persistence of HIV-1 in expanded cytotoxic T cell clones, Immunity (2022), https://doi.org/10.1016/j.immuni.2022.03.004

Single-cell recursive feature elimination and random forest validation (scRFE)

To identify key features that differentiate clones containing HIV-1 RNA$^+$ cells and clones without HIV-1 RNA$^+$ cells, we employed single-cell identity definition using random forests and recursive feature elimination (scRFE, version 1.5.6) (Park et al., 2020) with a bootstrapping modification. Briefly, this method trained a binary random forest classifier between two groups. These groups were artificially set to be of equivalent size prior to model training. After each training, features were ranked by importance and the least important features were removed. After several iterations, a core set of markers was identified that is necessary and sufficient to differentiate the two groups. Due to the extreme imbalance of our dataset, we additionally performed 10,000 replicates of scRFE. Results of all replicates were then aggregated to select the 200 features consistently selected by scRFE. This process was completed independently for all cells, cells only from the viremic time point, and cells only from the suppressed time point. These 200 features identified from all cells were validated in a subsequent model on the whole dataset. First, data were split into training and test sets (80–20), then Synthetic Minority Oversampling Technique (SMOTE (Chawla et al., 2002), Imbalanced-learn (Lemaître et al., 2017)) was used to generate artificial samples for the minority class in only the training dataset. A random forest classifier was then trained with default parameters except for a min_samples_leaf parameter of 16, oob_score set to true, and an nEstimators parameter of 100. Model performance was evaluated using the test set for both area under the receiver operating characteristic (AUROC) and F1-score weighted toward recall.

Pathway enrichment analysis

Genes were ranked using average log fold change in gene expression comparisons between groups. Genes were ranked using Pearson correlations with clone size. The resulting gene ranks were used to run pre-ranked gene set enrichment analysis as implemented by fGSEA (version 1.16.0)(Korotkevich et al., 2019). Human gene sets H (“hallmark”), C2 (“curated”), C6 (“oncogenic”), and C7 (“immunologic”) were used, version 7.4 (Liberzon et al., 2011). Gene sets were considered significantly enriched with an adjusted *P* value less than 0.05. To identify gene ontology pathways with a specific set of genes, we utilized Enrichr (Chen et al., 2013).

To identify differentially expressed gene sets and the upstream regulators of the transcription profile, ingenuity pathway analysis (IPA, Summer 2021 release, QIAGEN) (Krämer et al., 2014) was performed using gene expression log fold change cutoff of 0.25 or a non-zero coefficient where applicable. Analysis was performed with default settings.

QUANTIFICATION AND STATISTICAL ANALYSIS

Unless otherwise noted, statistical analysis was performed using R (version 4.0.3). Multiple hypothesis correction was applied where applicable using the method described by Benjamini-Hochberg (Benjamini and Hochberg, 1995).